LEAD ARTICLE

Acta Cryst. (1994). A**50**, 658–685

Structure Relationship to Dielectric, Elastic and Chiral Properties

BY S. C. ABRAHAMS

Physics Department, Southern Oregon State College, OR 97520, *USA*

(*Received* 5 *April* 1994; *accepted* 23 *May* 1994)

Abstract

Crystallography provides a major approach toward reaching an understanding of the relationship between crystal structure and material physical properties. The specific relationships of five highly structure dependent physical properties, namely piezoelectricity, pyroelectricity, ferroelectricity, ferroelasticity and optical activity, to atomic arrangement are developed in this *Lead Article*. The major attributes of each property, together with the structural measurements required to establish the property–structure relationship, are introduced and illustrative results for each are given. Predictive criteria that emphasize the insight leading to new property–structure relationships are presented as is an expanded experimental access to the crystallographic study of materials.

I. Introduction

Considerable progress has been made in recent years towards understanding the nature of various physical properties in terms of the underlying crystal structure, leading to the suggested title *Crystal structures and physical properties* when this *Lead Article* was invited. There are many physical properties of the solid state, some of which are strongly structure sensitive whereas others are more directly related to the electronic distribution. In selecting a set of properties to review, an exercise necessary both for presentation coherence and space considerations, primary weight was given to those property–structure relations that would contribute most in stimulating an awareness of the insight that careful structural studies offer in understanding and predicting physical properties.

Among the physical properties most clearly related to the underlying crystal structure and for which an understanding of the relationship between property and structure has developed strongly over the last several decades are several major dielectric and elastic phenomena; in addition, considerable advances have been made more recently in elucidating the relationship between optical activity and structure. This article hence concentrates on the relationship of piezoelectricity, pyroelectricity, ferroelectricity, ferroelasticity and optical activity to crystal structure. Following an introduction to each property sufficient for the informed reader to start making original contributions in the field, the relational principles between property and structure are developed. Many of the illustrative examples selected in this *Lead Article* have inevitably been taken from studies best known to the author; where available, more general sources in the literature are additionally provided.

Optical properties including electrooptic, nonlinear optic* and photoelectric effects; transport properties including band gap, mobility, thermoelectricity, and thermal and electric conductivity; and such magnetic properties as diamagnetism and paramagnetism, among many others, while of great interest and although governed by crystal symmetry are less directly structure related and will not be considered further in this *Lead Article*. The structural origin of superconductivity has been sought for decades, with greatly renewed emphasis since the discovery of the high-transition-temperature cuprate perovskites but with success that remains limited. Consideration of the structural basis for a number of other important physical properties has also been eliminated here for reasons of space.

In addition to providing the stimulus outlined above, this article aims at fostering a stronger interest in explor-

Professor S. C. Abrahams has long been interested in the detailed relationship between the physical properties of crystals and their accurately measured atomic arangements. His neutron and X-ray automatic diffractometer designs in the late 'fifties and early 'sixties, used for many structure determinations, helped lead the subsequent shift to higher-accuracy measurement from that available with the photographic and manual diffractometer methods then prevalent. He has been concerned over the years with improving the application of statistical methods to crystallographic measurement. Distinguished member of technical staff at AT&T Bell Laboratories until his retirement, he was Humboldt-Forschungspreisträger at Universität Tübingen 1989–1990 *and is now Adjunct Professor at Southern Oregon State College. He was Editor of Acta Crystallographica* 1978–1987, *and has been Chairman of the IUCr Commission on Crystallographic Nomenclature since* 1978.

* An earlier *Lead Article* by Bailey, Cruickshank, Pugh & Sherwood (1991) considers the influence of molecular structure modifications on second-harmonic-generation efficiency.

ing the rewarding boundary between crystallography and all structure-dependent properties as well as encouraging a more comprehensive experimental approach to materials studied by traditional crystallographic methods.

II. Piezoelectricity

1. *Property description*

The 1880 discovery of piezoelectricity in quartz by Pierre and Jacques Curie followed an earlier speculation by C. A. de Coulomb that electricity might be produced in some crystals by pressure, and the work of Abbé R.-J. Haüy and later A. C. Becquerel who reported finding some electrical effects when certain crystals including calcite were compressed, although these were subsequently attributed primarily to contact electricity (see Cady, 1964). Piezoelectricity remained only a matter of academic interest until the property was put to use in World War I in submarine echo location devices. The direct piezoelectric effect is the production of an electric polarization in a material by the application of stress; the converse effect is the formation of a strain by the application of an electric field. Soon after the war, W. G. Cady invented the piezoelectric resonator, in which a piezoelectrically driven mechanical resonance in a quartz crystal interacts with the electrical driving circuit, thereby permitting frequency control of an electrical oscillator. During the following decades, piezoelectric materials came into widespread technological use in the form of single crystals (both mineral and synthetic), ceramics and polymers.

Initially used as filters, oscillators and frequency standards, piezoelectric applications broadened into audiotransducers, delay lines and actuators, and later accelerometers, fuses, phonograph cartridges, tweeters, sonar generators, ultrasonic processors, acoustic surface-wave devices, acoustic microscopes and light-diffracting acoustic gratings, among others [for additional applications, see Burfoot & Taylor (1979); Abrahams & Nassau (1986)].

2. *The direct piezoelectric effect*

The application of a stress σ_j along an appropriate jth direction produces an electric polarization P_i in a piezoelectric material, as given by

$$P_i = d_{ij}\sigma_j, \tag{1}$$

where i has values 1, 2, 3 for the polarization produced along the crystal a, b, c directions, j has values 1, 2, 3 for tensile (or compressive) stress applied along a, b, c directions and values 4, 5, 6 for shear stress about bc, ca, ab, and d_{ij} are the piezoelectric strain moduli relating the ith and jth directions. The additional subscript required for third-rank tensors is no longer in general use for the piezoelectric moduli since d_{ijk} is symmetric in j and k (*cf.* Nye, 1957; *International Tables for Crystallography*, 1994). It may be seen from (1) that the sign of the polarization produced by a tensile stress along a given piezoelectrically active crystal direction is reversed if replaced by a compressive stress. If the crystal possesses a spontaneous polarization P_s, then it is the change produced in P_s (*i.e.* ΔP_s) that becomes proportional to the stress, see also § V.2.

3. *The converse piezoelectric effect*

The application of an electric field E_i along an appropriate direction j produces a strain ε_j in a piezoelectric material, as given by

$$\varepsilon_j = d_{ij}E_i \tag{2}$$

with piezoelectric coefficients d_{ij} identical to those in (1). These d_{ij} are often reported as strain coefficients and have been measured for many piezoelectric materials. Their magnitudes, which range from 10^{-8} to 10^{-3} C N^{-1}, are generally temperature dependent; both maxima and minima in their dependence have been reported. A systematic collection of coefficient magnitudes and the corresponding thermal coefficients for many piezoelectrics may be found in Landolt-Börnstein (1984).

4. *Piezoelectric moduli*

All noncentrosymmetric crystal classes are piezoelectric except for class 432, in which the moduli of all d_{ij} are zero. The full set of 18 nonequivalent coefficients are present in triclinic class 1. The number of nonequivalent d_{ij} moduli in the remaining 19 crystal classes ranges from 10 in class m to 1 in classes 422, 622, $\bar{6}m2$, $\bar{4}3m$ and 23 (see Nye, 1957), as a consequence of some moduli having zero value or being equivalent to others.

It is customary to use orthogonal x, y and z crystal axes as the basis for d_{ij} moduli identification. The *IEEE Standard on Piezoelectricity* (1978) convention takes the first of the nonzero coefficients d_{33}, d_{11}, d_{22}, d_{36} or d_{31} as positive; in the case of d_{33}, for example, a positive value is taken to mean that tensile stress applied along the z axis will result in the generation of a potential difference between the ends of this axis with (001) as the positive terminal. The sense of the second axis is similarly determined as positive by applying the same rule to the next nonzero coefficient in the group. The sense of the third axis follows by maintaining a right-handed system. A ready means of applying tensile stress is by releasing an applied compressive stress. It may be noted that, whereas the signs of all elastic moduli are the same for left- and right-handed crystals, all piezoelectric moduli have opposite signs for left- and right-handed crystals.

Experimental measurement of the moduli magnitudes may be made on small single crystals by a variety of methods (*cf.* Mason & Jaffe, 1954). The simplest is a static measurement of the direct effect, although the converse effect (in which the change in crystal shape is measured as a function of the applied electric field) is generally more accurate. In the former, a crystal plate is prepared with major faces normal to the piezoelectric *j*th direction, then electroded and connected to an electrometer. Compressive stress may be applied *via* an insulating rod as the sign and magnitude of the polarization produced is measured in coulombs [see, for example, Abrahams (1975)]. The magnitude of the compressive stress is readily determined either by using a known mass and crystal face area or by means of a calibrated spring-loaded device (*cf.* Abrahams & Bernstein, 1979).

5. *Absolute sense of piezoelectric moduli*

Determination of the absolute atomic arrangement (*i.e.* the arrangement with respect to any macroscopic physical property) in a piezoelectric crystal on the basis of an anomalous-scattering measurement [it may be noted that *International Tables for Crystallography* (1992) proposes dropping the term 'anomalous scattering' in favor of the preferable term 'dispersion'] allows the absolute sense of one or more d_{ij} coefficients to be determined, since all signed crystal tensor properties are absolute with respect to structure. A survey of experimental diffraction methods for the determination of signed crystal tensor moduli has been presented (Abrahams, 1975). Particular care is necessary in measuring the absolute sense of a given modulus. The diffraction results must be unambiguously related to the physical measurements, preferably by using the same crystal for both sets. Absolute determinations of sign are, by their nature, necessarily either right or wrong, see also § XI.1.

In any given crystal, since the *IEEE Standard on Piezoelectricity* (1978) convention is as likely to disagree with the absolute sense as agree, conformity with the convention is readily maintained by reversing the arbitrarily assigned sense of the corresponding crystal axis if necessary, while ensuring that the remaining axes continue to form a right-handed system. Although the magnitudes of the d_{ij} moduli have been measured for many hundreds of crystals (see, for example, Landolt-Börnstein, 1984), the absolute signs have been determined for no more than about 10% of them.

III. Structure and piezoelectricity

1. *Internal crystal response to external stress*

The relationship between structure and piezoelectricity in a given material is most readily visualized by considering several inorganic materials for which the absolute moduli have been determined. In each case, the polarization resulting from an induced structural distortion produced by the application of a stress field is considered in relation to the absolute orientation of the crystal axes. The first two piezoelectrics, ZnO in point group $6mm$ and chalcopyrite in $\bar{4}2m$, are comprised of infinitely connected diamond-like tetrahedral atomic arrangements without individual ionic groups. By contrast, piezoelectric α-$LiIO_3$ in point group 6 contains individual ionic groups. The final example chosen, low-quartz* in point group 32, again has an infinitely connected tetrahedral atomic arrangement. An external application of stress to crystals of ZnO, $ZnGeP_2$, $AgGaS_2$ or low-quartz is accompanied by an internal response of bond strength to compression or dilation with magnitude determined by the relative ease with which the bond angles deform. In the remaining case, accommodation to the external application of stress occurs primarily through the variation in electrostatic interaction between rigid ions that results under stress. The absolute polarization produced in a piezoelectric crystal may be related directly to the structural distortion caused in each unit cell on the basis of the consequent change in point-charge distribution.

2. *Piezoelectric and pyroelectric hexagonal* ZnO, *zincite*

Among the first crystals to be analyzed by X-ray diffraction (Bragg & Bragg, 1915) and that later became the subject of numerous structural reinvestigations, ZnO is found to crystallize in space group $P6_3mc$ with $a = 3.249\,858\,(6)$ and $c = 5.206\,619\,(2)$ Å at 298 K [Barns (1968), as quoted by Abrahams & Bernstein (1969)]. The absolute piezoelectric strain moduli $d_{31} = -5.43$, $d_{33} = +11.67$, $d_{15} = -11.34\,\mathrm{pC\,N^{-1}}$ are taken from Landolt-Börnstein (1984). The experimental observation by Heiland, Kunstmann & Pfister (1963), among others, that the (001) face develops a negative charge under compressive stress applied along the polar [001] axis for this structure with sole variable atomic coordinate $z(\mathrm{O}) \simeq 0.382\,5$ (Abrahams & Bernstein, 1969) provides the basis for the absolute assignment of sense to d_{33}. The single positional parameter of this structure provides a simple example for illustrating the direct relationship between structure and piezoelectricity. The tetrahedron of O atoms about each Zn atom is oriented such that the normal from Zn to the triangular face of O atoms perpendicular to the polar axis is directed toward the positive end of the dipole formed under compressive stress along [001], as illustrated in Fig. 1. The *IEEE Standard on Piezoelectricity*, see § II.4, which assigns

* Low-quartz is the designation used by Donnay & Le Page (1978), among others, for the low-temperature phase of quartz. A recommended nomenclature for use in distinguishing the sequence of phases that a material may form as a function of temperature or pressure is currently under consideration by the IUCr Working Group on Phase Transition Nomenclature.

the d_{33} modulus a positive sense by convention, is hence in agreement with the absolute polarization observed in ZnO as shown in Fig. 1.

The structural origin for the absolute sense of d_{33} in hexagonal ZnO, assuming the charge on Zn is positive relative to the negative charge on O, lies in the difference between the compressive strength of the Zn–O bond and the deformation strength of the O–Zn–O bond angle. If, as expected, the former is greater than the latter, then compressive stress applied along the Zn–O bond parallel to [001] necessarily results in a displacement of the Zn atom toward the triangular O-atom face as the O–Zn–O angle made by these three O atoms increases. As the positively charged Zn atom approaches this face [equivalent to $(00\bar{1})$] under compressive stress, the charge induced thereon is necessarily positive; the corresponding (001) face likewise becomes negative under compression and hence positive under dilation. The d_{33} modulus is thus structurally predicted to be positive, in agreement with observation.

The structural origin for the negative sense of d_{31} may be similarly derived. This modulus relates the polarization generated on (001) to tensile stress applied along an a axis. Compressive stress applied along $\mathbf{a}_1$ has no effect on the orientation of the Zn–O bond parallel to the polar axis but increases the O–Zn–O angle this bond makes with the three other Zn–O bonds. This angular increase results in all three bonds inclined to [001] projecting a larger dipole component along **c**, thereby producing a positive polarization on the (001) face. Conversely, tensile stress along $\mathbf{a}_1$ produces a negative polarization on (001), in agreement with the negative sign measured for the d_{31} modulus. The pyroelectric properties of ZnO are discussed in § V.2.

3. *The piezoelectric tetragonal* $ZnGeP_2$ *and* $AgGaS_2$ *chalcopyrite family*

Numerous materials with formula $A^{II}B^{IV}C^{V}_2$ or $A^{I}B^{III}C^{VI}_2$, where the superscripts denote respective groups in the Periodic Table, crystallize with the chalcopyrite-type structure and exhibit technologically useful optical, piezoelectric and semiconducting properties (*cf.* Shay & Wernick, 1974). Each atom in the chalcopyrite structure, with space group $I\bar{4}2d$ [$AgGaS_2$ at 298 K for example has a = 5.757 22 (3), c = 10.303 6 (2) Å (Abrahams & Bernstein, 1973)], is tetrahedrally bonded; as for the ZnO structure, see § III.2, chalcopyrite is characterized by a single structural parameter. In case all tetrahedra are regular, the interatomic dipoles exactly cancel; otherwise, each tetrahedron is associated with a small residual dipole. Each tetrahedral dipole is necessarily cancelled exactly by an identical but opposing dipole within the unit cell in the case of zero applied field. However, the $d_{14} = d_{25}$ and d_{36} moduli are nonzero in this point group and hence shear stress in the basal plane (normal to **c**), for example, leads to a deformation of the tetrahedra and a resulting polarization on the (001) face.

Experimentally, the absolute sense of $d_{14} = d_{25}$ and d_{36} has been determined as positive both in $ZnGeP_2$ and in $AgGaS_2$ (Abrahams, Barns, Bernstein & Turner, 1974) by combining use of the extended-face X-ray dispersion method [see Abrahams (1975) for a survey of different methods] and measurement of the electrostatic charge that develops on that extended face under tensile stress. The relationship between atomic arrangement and absolute moduli is illustrated in Fig. 2. It may be seen that tensile stress along [110] tends to increase the separation between A and B atoms at (0,0,0) and $(\frac{1}{2},\frac{1}{2},0)$, thereby displacing the C atom at $(x,\frac{1}{4},\frac{1}{8})$ toward $(00\bar{1})$. If it is assumed that the C atom in both chalcopyrites forms the negative dipole end of the sulfur–metal (or phosphorus–metal) bond, then it is apparent that tensile stress must result in the development of a positive

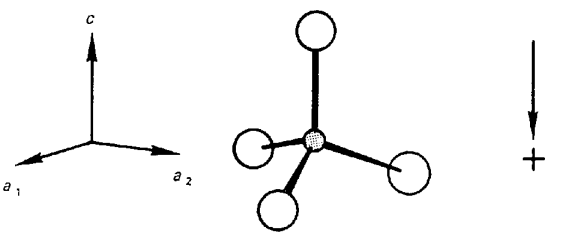

Fig. 1. Absolute spatial relation of a ZnO_4 tetrahedron in ZnO to the polarization induced by compressive stress applied along **c**, after Abrahams & Bernstein (1969). The shaded circle represents Zn, the open circles O.

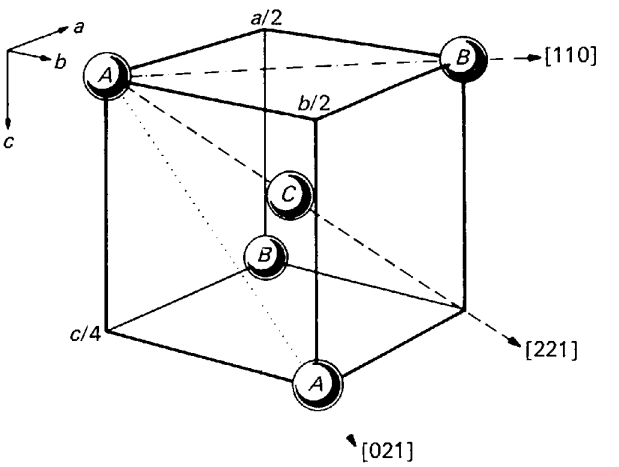

Fig. 2. Absolute spatial relation of the A, B and C atoms in part of the chalcopyrite unit cell ($a/2 \times b/2 \times c/4$), illustrating the tetrahedron of A and B atoms about each C atom. Tensile stress along [110], shown as a dot-dashed line, causes a positive polarization on (001). Tensile stress along [221], shown as a dashed line, causes a positive charge on (112). Tensile stress along [021], shown as a dotted line, causes a positive charge on (100). After Abrahams, Barns, Bernstein & Turner (1974).

polarization on (001), in agreement with the positive sign found experimentally for d_{36}. As noted in § II.4, the *IEEE Standard on Piezoelectricity* calls for a choice of crystal axes such that d_{36} is positive in the absense of experimentally measured absolute moduli, in agreement with the absolute determinations in these chalcopyrites.

The absolute sense of d_{14}, also experimentally found to be positive in the same study, may be similarly related to the crystal structure by considering Fig. 2. Tensile stress along [021] clearly results in a displacement of the *C* atom toward the $(\bar{1}00)$ face, hence producing a positive polarization on (100) as expected for $d_{14} > 0$.

Comparable results are found for the zinc-blende structures CuCl and ZnS (Miller, Abrahams, Barns, Bernstein & Nordland, 1971), for which $d_{14} = d_{25} = d_{36} > 0$ in point group $\bar{4}3m$. The relationship of these absolute moduli to the atomic arrangement may also be illustrated by reference to Fig. 2, in which the *A* and *B* atoms are taken as identical in a cubic unit cell with $a \simeq 5.41$ Å. Displacement of the negative *C* atom (Cl or S) toward $(00\bar{1})$ under tensile stress applied along [110] clearly produces a positive polarization on (001), in agreement with experiment.

4. *Piezoelectric and pyroelectric hexagonal α-lithium iodate*

Unlike the tetrahedral structures in §§ III.2 and III.3, α-$LiIO_3$ contains discrete Li^+ and IO_3^- ions in a hexagonal cell with $a = 5.481\,27\,(7)$, $c = 5.171\,65\,(8)$ Å at 295 K and space group $P6_3$ (Svensson, Albertsson, Liminga, Kvick & Abrahams, 1983). The independent moduli are $d_{31} \simeq 4$, $d_{33} = +46$, $d_{14} \simeq 7$ and $d_{15} \simeq 49$ pC N^{-1}; the absolute sense has been measured only for d_{33} (Landolt-Börnstein, 1984). Rosenzweig & Morosin (1966) and Morosin (1972; see Bergman & Crane, 1974) reported that the apexes of the pyramidal IO_3^- ions point in the same direction as the more steeply pointed ends of α-$LiIO_3$ crystals, the ends that also develop a positive polarization under tensile stress applied along the polar axis. Svensson *et al.* (1983) and Abrahams, Liminga & Albertsson (1990) have confirmed the earlier reports which had been disputed, see § V.3. Each IO_3^- ion with its three 1.808 Å I–O bonds is associated with three additional I–O bonds longer than about 2.9 Å. Fig. 3 presents the absolute orientation of the content of one unit cell, showing the three longer (dashed) I–O bonds that complete the distorted octahedron about iodine and also the six Li–O contacts.

The Li–O contacts are of approximately equal length, at about 2.14 Å, and may be taken as equally deformable but the longer I–O bonds are more readily deformable than the shorter I–O bonds. Compressive stress applied along **c** allows a parallel displacement component relative to I only by the Li^+ ions if the IO_3^- ion is rigid, to first order; the IO_3^- ion may only rotate about the sixfold axis under such stress. In consequence, [001] tensile stress results in an Li^+-ion displacement toward (001), thereby leading to a positive polarization on that face (*i.e.* $d_{33} > 0$) in accordance with observation (Liminga & Abrahams, 1976).

5. *Piezoelectric hexagonal α-quartz*

The piezoelectric properties of α- or low-quartz (see footnote to § III.1) have made such an important contribution to modern technology, in the form of crystal oscillators, that the briefest of surveys should include this material. The α-quartz crystal oscillator circuit frequency of 2^{15} Hz, controlled to generate second-, minute- and hour-duration pulses and providing an accuracy better than 1 min per year, is widely distributed not only in clocks and watches but also in most equipment that depends on accurate time division.

The abundant confusion in the earlier literature settings used for α-quartz, with lattice symmetry $6/m\,2/m\,2/m$ and crystal point group 321, has been thoroughly addressed by Donnay & Le Page (1978). The 1978 *IEEE Standard on Piezoelectricity* follows their recommendation by eliminating the earlier unique convention for quartz. α-quartz is thus to be described only in space group $P3_121$ with a right-handed coordinate system (RHCS) in the $r(+)$ crystal setting: the setting $r(+)$ denotes a crystal orientation for which the morphologically major rhombohedron *r* is indexed $\{10\bar{1}1\}$ and the twofold axis along which the 0*x* coordinate axis is chosen develops a positive (+) charge at its positive end under tensile stress. The crystal structure determination by Le Page, Calvert & Gabe (1980) of a (laevorotatory) crystal with a structural right-handed screw axis in the RHCS satisfies this convention.

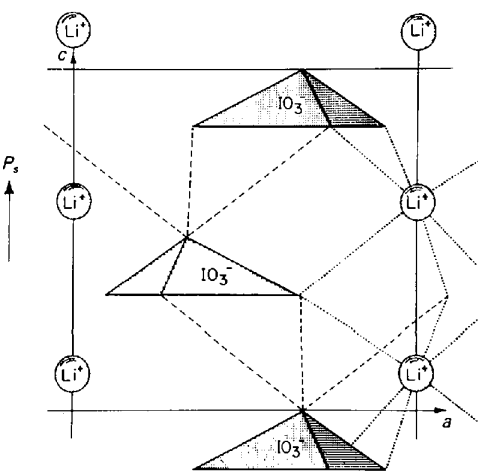

Fig. 3. Absolute orientation of IO_3^- and Li^+ ions in α-$LiIO_3$. The positive sense of the *c* axis points toward the more steeply pointed ends of crystals grown from aqueous solution. Tensile stress along [001] produces a positive polarization on (001), as does heating. The long I–O bonds are shown as dashed lines, the Li–O bonds as dotted lines (after Liminga & Abrahams, 1976).

The two independent absolute moduli $d_{11} = -2.27$ and $d_{14} = -0.90\,\text{pC N}^{-1}$ are as listed for a laevorotatory crystal in Landolt-Börnstein (1984); the signs for both moduli are the reverse of those for a dextrorotatory crystal, see § II.4. The relationship of crystal chirality to optical activity is discussed in §§ X and XI. Point group 321 is not pyroelectric, see § IV.4.

Le Page, Calvert & Gabe (1980) showed that the slightly distorted SiO_4 tetrahedron remains virtually rigid on heating from 94 to 298 K, with a rotation over this range of ~0.8° as the Si–O–Si angle between corner-linked tetrahedra increases by ~1.0°. The distortion from tetrahedral regularity is small, with the two independent Si–O bond lengths in each of the three tetrahedra per unit cell differing only by 0.005 Å and the Si atom displaced only by 0.002 (1) Å from the mass center of its four bonded O atoms. The corresponding change in lattice parameters over this 204 K thermal interval is about 0.2%. The considerations that follow show that rotation of the rigid tetrahedra under tensile stress cannot explain the order of magnitude of the observed piezoelectric moduli. With the assumption, for simplicity, of unit elementary charge separation between Si and O, the resulting electric dipole for each tetrahedron is $\sim 3 \times 10^{-32}$ C m directed along the appropriate a_1, a_2 or a_3 axis: the three together symmetrically cancel under zero applied stress. The magnitude of this dipole is two orders of magnitude smaller than that of H_2O, for example. The net polarization on (10.0) resulting from tensile stress applied along the diad [10.0] axis, if the tetrahedra rotate rigidly under stress by an angle comparable to the maximum observed on heating, is hence on the order of 1% of $\sim 3 \times 10^{-32}$ C m; this very small value would give rise to a negligible polarization with resulting $d_{11} \simeq 0$. The small angular rotation assumption is entirely consistent with the strain produced by application of finger pressure to an α-quartz crystal (see § III.6): with elastic compliances in the range $-1 < c_{ij} < 20 \times 10^9\,\text{N m}^{-2}$, the calculated strain is on the order of 10^{-5}. The only alternative for the sense and magnitude of the observed d_{11} modulus thus lies in an increased tetrahedral distortion under applied stress.

Examination of Le Page, Calvert & Gabe's (1980) results show that the two shorter 1.606 Å Si–O bonds in each tetrahedron are oriented nearly parallel to a pair of (10.0), (01.0) or (11.0) planes. Tensile stress applied along [10.0] may hence be expected to distort the two SiO_4 tetrahedra that have an Si–O bond nearly parallel to (10.0) by decreasing three of the O–Si–O angles in each tetrahedron from their equilibrium value of ~109.5° to give a negative polarization at (10.0), in agreement with the negative d_{11} modulus observed. The third tetrahedron contributes only to tensile stress along [01.0] or [11.0]. Similarly, shear stress about the a_2 and c axes is also expected to distort the SiO_4 tetrahedra so as to produce a negative polarization at (10.0), consistent with the observed negative d_{14} modulus. Remeasurement of the α-quartz structure under stress, by the methods outlined in § III.8, is necessary to confirm the anticipated structural distortions.

6. *Piezoelectric atomic displacements*

The atomic displacement sense and magnitude produced in a piezoelectric crystal under a given tensile stress may be estimated from the absolute piezoelectric moduli, the absolute crystal structure and a model relating atomic distribution to macroscopic polarization P_s. The point-charge model for an ionic crystal gives P_s by means of

$$P_s = (e/V)\sum_i Z_i d_i, \tag{3}$$

where e is the elementary charge $1.602\,2 \times 10^{-19}$ C, V is the unit-cell volume, Z_i is the charge on the ith ion and d_i is the component along the piezoelectric axis of the smallest charge separation. Dipolar contributions to P_s are treated by replacing the term $Z_i d_i$ in (3), for the i atoms involved, by the magnitude of the electric dipole D_i.

α-$LiIO_3$ provides a simple but typical example with $d_{33} = +46 \times 10^{-12}\,\text{C N}^{-1}$ and the structure shown in Fig. 3. The only displacements along the polar c-axis direction, within the unit cell, are those of Li^+ with respect to the IO_3^- ions for zero thermal expansion. The IO_3^- ions may rotate only about an axis parallel to **c**, hence tensile stress along [00.1] causes an Li^+-ion displacement toward (00.1) from the nearest layers of iodine atoms, generating a positive polarity on (00.1) in accordance with the positive modulus sign. Since moderate finger pressure on a 1 mm^2 area produces a stress on the order of $5 \times 10^6\,\text{N m}^{-2}$, it is convenient to consider the atomic displacements caused by a stress of $10^6\,\text{N m}^{-2}$. In α-$LiIO_3$, this stress would change the polarization by $46 \times 10^{-6}\,\text{C m}^{-2}$; the resulting Li^+-ion displacement, on the basis of (3), is thus about 1.9×10^{-4} Å/$10^6\,\text{N m}^{-2}$.

Estimates of the atomic displacements in other piezoelectric crystals range from about 0.1 to 3×10^{-4} Å/$10^6\,\text{N m}^{-2}$ (Abrahams, 1978).

7. *Structural predictions from absolute moduli*

All noncentrosymmetric crystal classes except for cubic 432 are piezoelectric. The accuracy of structure determinations in these classes is always improved if the dispersion component in the structure amplitudes is correctly treated, see § II.5. Such a treatment can lead to an assignment of the absolute sense of the crystal axes. Any assignment made only with respect to the diffraction experiment is necessarily inconclusive, whereas one made with respect to crystal morphology or

other physical property may be used by the diffractionist or others to determine the absolute piezoelectric moduli.

The absolute sense of one or more d_{ij} moduli may readily be measured if crystals with linear dimensions of about 2 mm or more are available. Once the absolute sense of the crystal axes in such a crystal has been determined it is, in principle, necessary only to connect electrodes from the pair of crystal faces terminating the ith-axis direction to an electrometer. Gentle pressure applied along the ith direction by means of an insulating rod then produces a polarization that is often on the order of $10^{-6}\,\mathrm{C\,m^{-2}}$ or greater. Rapid release of compressive stress, the equivalent of tensile stress application, following the onset of equilibrium within the crystal as measured by the electrometer will result in the opposite polarization sense and will thereby confirm the observed absolute sign of the modulus. Consideration of the absolute moduli can lead to greater structural insight than that available otherwise, as illustrated by the preceding sections.

It is clearly advisable to determine the absolute sense of one or more independent piezoelectric moduli for all new noncentrosymmetric structures reported if crystals of adequate size can be grown: alternatively, the absolute structure should be related at least to the crystal morphology. Use of the term 'absolute' in crystallographic reporting should be made with care, see previous section and also Glazer & Stadnicka (1989), for example.

8. *New piezoelectricity-structure probe*

A novel and potentially very fruitful range of experiments is now becoming feasible in which advantage is taken of high-intensity synchrotron X-radiation as a probe of the structural changes in piezoelectric crystals that result from applying stress or an electric field. Such experiments may be based either on the direct or the converse piezoelectric effect. In the former, reproducible compressive stress is readily applied to the sample crystal by using an attached piezoelectric transducer and a set of appropriate constraints. In the latter, the d.c. field is applied directly to the crystal by means of transparent electrodes (such as thin films of aluminium). In either case, the resulting atomic displacements necessarily modify the diffraction intensities. The intensity distribution corresponding to the undisturbed structure and to the structure under the direct application of compressive stress, or to the structure under a compressive or tensile stress resulting from an applied d.c. field, may be measured by synchronously gating the detector and the voltage supply to the transducer in the direct effect or to the sample in the converse effect using techniques such as those described by Ståhl, Kvick & Abrahams (1990). The direct effect is simpler in principle, but the converse effect may lead to an easier experiment. In the latter, correction for electrostrictive and surface effects due to the electrodes may be necessary. Techniques such as those outlined are expected to open a series of field-induced structural changes to direct examination.

IV. Pyroelectricity

1. *Property description*

Pyroelectric materials characteristically develop an electric polarization as the temperature is changed. All pyroelectric materials are also piezoelectric; some are in addition ferroelectric, see § VI, although the converse does not necessarily apply. The polarization produced in a pyroelectric material heated by a wide energy range of radiations, from the far infrared to beyond the ultraviolet, has led to widespread use of the property in an array of devices including infrared detectors, temperature sensors, motion sensors, calorimeters, thermal imagers and pyroelectric vidicon tubes. An atomic basis for the origin of this property, first observed over 23 centuries ago by Theophrastus as an attractive power in tourmaline when heated (Lang, 1974), is hence of value both fundamentally and technologically.

2. *Primary pyroelectricity*

A polarization change ΔP_i is produced in a pyroelectric crystal subjected to uniform heating: as noted in § IV.4, all pyroelectric crystals possess a temperature-dependent spontaneous polarization P_s. A temperature change ΔT produces a proportional change ΔP_i in P_s as given by

$$\Delta P_i = p_i \Delta T, \tag{4}$$

where p_i is the pyroelectric coefficient along the ith crystal-axis direction. In principle, ΔP_i is observable in two different ways. In one, the shape and size of the crystal may be held constant by suitable application of constraints, *i.e.* at constant strain; in the other, the crystal is held free and is allowed to undergo normal thermal expansion, *i.e.* at constant stress. The first case corresponds to primary (or true) pyroelectricity; an additional effect arising from a piezoelectrically induced polarization change, namely secondary pyroelectricity, is present in the second case. The normal, and simplest, experiment measures pyroelectricity in an arrangement that corresponds to the second case, leading to a sum of the two effects. Nonuniform heating with its resulting thermal gradients may cause nonuniform stresses and strains and may thereby result in tertiary or false pyroelectricity through piezoelectric effects. Such effects are best eliminated experimentally to avoid the production of false results. Secondary pyroelectricity is treated in the following section.

3. *Secondary pyroelectricity*

The polarization produced in a pyroelectric crystal that is free to deform and that is additional to the primary pyroelectricity produced by a temperature change in a crystal of fixed shape and volume is referred to as secondary pyroelectricity. The ratio of the primary (p_i') to the secondary (p_i'') pyroelectric coefficient in a given crystal ranges from about 10^{-1} to 10^2 (Landoldt-Börnstein, 1984). The pyroelectric coefficient is a vector quantity, and the sign of the primary coefficient may differ from that of the secondary coefficient at a given temperature.

4. *Pyroelectric moduli*

The spontaneous polarization P_s and the pyroelectric coefficients p_i conform to the symmetry of the crystal point group, and are nonzero only in the ten noncentrosymmetric groups for which a direction exists that is not repeated by any symmetry element. A pyroelectric point group may hence possess no more than a single axis of symmetry nor any mirror other than those parallel to the unique axis (*International Tables for Crystallography*, 1994). The subscript $i = 1$, 2 or 3 corresponds respectively to the a, b or c crystal axis for all point groups with a unique direction, in which case a single coefficient p_i suffices. P_s and p_i may lie along any direction in the mirror plane of point group m and hence is characterized there by two p_i components; in point group 1, the pyroelectric vector may assume any direction within the unit cell whence it therefore has three p_i components. The magnitude of the combined primary and secondary coefficients p_i in nonferroelectric pyroelectrics ranges from about 10^{-8} to $10^{-3}\,\mathrm{C\,m^{-2}\,K^{-1}}$ and in ferroelectric pyroelectrics from about 10^{-6} to $10^{-2}\,\mathrm{C\,m^{-2}\,K^{-1}}$ (Landolt-Börnstein, 1984).

Quantitative measurement of the moduli may be made by static, dynamic and indirect methods; a review is given in Landolt-Börnstein (1984). A common technique in which a radiant light source heats the crystal and a charge-integration amplifier collects the resulting pyroelectric charge is based on a method pioneered by Glass (1969). The total coefficient p_i generally exhibits a nonmonotonic characteristic temperature dependence that may have several maxima or minima resulting from the separate thermal dependence exhibited by the component primary and secondary coefficients; the total temperature dependence may be of either sign.

5. *Absolute pyroelectric moduli*

The positive sense of P_s and hence of p_i is generally taken as coincident with the positive axial sense given by the 1978 *IEEE Standard on Piezoelectricity*, see § II.4, although the sign of p_i is not commonly reported in the literature. While use of the IEEE convention is preferable to neglecting the sign, greater insight is provided by measuring the pyroelectric coefficient sense in terms of the absolute atomic arrangement to give its absolute vector sense or polarity. Experimental measurement of the absolute polarity is readily made if single crystals with all dimensions greater than about 1 mm are available, *i.e.* the absolute polarity is more easily measured than are the absolute piezoelectric moduli. Following determination of the absolute sense of the crystal axes with respect to the structure, see § II.5, it is necessary only to connect the electroded crystal surfaces normal to the ith unique direction to an electrometer and then raise the temperature of the shielded crystal by ΔT. A calibrated pulse from the radiant source (see preceding section), which results in a known ΔT along the ith direction within the crystal sample, thus produces a polarization with a measurable magnitude and a sense that reverses as the crystal cools, thereby giving the absolute pyroelectric coefficient p_i.

V. Structure and pyroelectricity

1. *Internal crystal response to temperature change*

The relationship between structure and pyroelectricity is considered in three simple inorganic nonferroelectric pyroelectrics in the following sections. The spontaneous polarization in pyroelectric crystals originates partly in the ionic and partly in the electronic charge distributions. The temperature dependence of the latter are neglected in this paper. The first example below is ZnO in point group $6mm$, the second is α-$LiIO_3$ in point group 6 and the last to be examined is $Li_2SO_4{\cdot}H_2O$ in point group 2. The absolute structure of ZnO has already been discussed in § III.2 and that of α-$LiIO_3$ in § III.4, each with respect to the production of piezoelectricity: their structures are again taken up to illustrate the origin of pyroelectricity in terms of the atomic displacements. The detailed investigation of both the primary and secondary pyroelectric coefficient temperature dependence in $Li_2SO_4{\cdot}H_2O$ by Lang (1971, 1974) led to its selection as the third example.

2. *Pyroelectric and piezoelectric hexagonal* ZnO, *zincite*

This material, considered in § III.2 to illustrate the relationship between piezoelectricity and atomic arrangement in a simple structure, also illustrates the relationship between pyroelectricity and structure rather clearly since the production of primary pyroelectricity in ZnO is due entirely to the thermal displacement of oxygen relative to the location of zinc in the unit cell whereas the secondary coefficient is due to the polarization produced by thermal expansion. The total pyroelectric coefficient (p_3) of ZnO has been measured at room temperature as $-9.4 \times 10^{-6}\,\mathrm{C\,m^{-2}K^{-1}}$, with a magnitude that varies between $-0.28 \times 10^{-6}\,\mathrm{C\,m^{-2}\,K^{-1}}$ at 20 K and about

$-11 \times 10^{-6}\,C\,m^{-2}\,K^{-1}$ at 500 K (Landolt-Börnstein, 1984). The secondary pyroelectric coefficient (p_3'') at 300 K may be calculated from the piezoelectric stress (e_{ij}) and thermal-expansion (α_j) coefficients for ZnO as $-5.2 \times 10^{-6}\,C\,m^{-2}\,K^{-1}$ from the relation $p_3'' = 2e_{31}\alpha_1 + e_{33}\alpha_3$. The total coefficient value thus gives the primary pyroelectric coefficient, by difference, as $p_3' = -4.2 \times 10^{-6}\,C\,m^{-2}\,K^{-1}$ at room temperature.

The ZnO structure has been studied by neutron diffraction over a wide temperature range (Albertsson, Abrahams & Kvick, 1989). The resulting oxygen-displacement thermal-dependence linear coefficient between 20 and 900 K has thereby been determined at $0.263\,(8) \times 10^{-4}\,\text{Å}\,K^{-1}$ with respect to the fixed Zn atom taken as origin. A direct relationship between atomic displacement and primary pyroelectric polarization of -0.063×10^{-4} Å/$10^{-6}\,C\,m^{-2}$ is hence established in ZnO. The same study provided accurate values for the α_1 and α_3 linear thermal-expansion coefficients used above to evaluate p_3''.

The absolute primary pyroelectric polarization P_s may also be calculated directly from the structure determined at each measurement temperature. The model used assumes an equal but opposite point charge q at the Zn and O sites that is invariant with temperature, and also assumes that any electronic redistribution with temperature is negligible. The tetrahedron of O ions [at $(1/3, 2/3, z)$] about zinc [at $(1/3, 2/3, 0)$] in space group $P6_3mc$ is distorted and may be shown to have a net polarization along the positive c axis of $-(16z-6)q/(3)^{1/2}a^2$ for a complete unit cell. The resulting calculated values of $P_s(300\,K) = -6.00\,(10) \times 10^{17} q\,m^{-2}$, $P_s(600\,K) = -6.91\,(23) \times 10^{17} q\,m^{-2}$ and $P_s(900\,K) = -7.89\,(23) \times 10^{17} q\,m^{-2}$ suggest a rather linear thermal dependence for the polarization between 300 and 900 K, with average calculated $\Delta P_s/\Delta T = -3.2\,(6) \times 10^{14} q\,m^{-2}\,K^{-1}$. The primary coefficient $p_3' = -4.2 \times 10^{-6}\,C\,m^{-2}\,K^{-1}$ given above, together with the elementary charge e taken as $1.602\,2 \times 10^{-19}$ C and the average value of the calculated primary coefficient $\Delta P_s/\Delta T$, results in $q \simeq 0.1\,e$. It is notable that the magnitude of ΔP that develops over the full experimental 880 K temperature range arises from a total ionic displacement that is only about 0.023 Å, even for the small charges found on the Zn and O atoms. It may be noted further that, although the value of p_3' calculated from the diffraction measurements is in excellent agreeement with experiment at temperatures midway between the diffraction measurements [$-11\,(4)$ and $-10.3 \times 10^{-6}\,C\,m^{-2}\,K^{-1}$ at 450 K and $-11\,(5)$ and $-11.6 \times 10^{-6}\,C\,m^{-2}\,K^{-1}$ at 750 K, respectively], the value calculated at 160 K [$+1\,(2) \times 10^{-6}\,C\,m^{-2}\,K^{-1}$] departs significantly from experiment ($-6 \times 10^{-6}\,C\,m^{-2}\,K^{-1}$) owing, possibly, to the neglect of electronic redistribution at lower temperatures.

3. *Pyroelectric and piezoelectric hexagonal α-lithium iodate*

The relationship between pyroelectricity and structure is particularly illustrative in α-$LiIO_3$ for several reasons. The structure is simple, as shown in Fig. 3, and has been extensively investigated, as also has been its pyroelectric properties; in addition, α-$LiIO_3$ provides a useful cautionary example of the pitfalls associated with the assignment of absolute atomic configuration, polarity and crystal morphology. The crystal structure has been determined by neutron and X-ray diffraction at ten temperatures between 20 and 500 K (Svensson, Albertsson, Liminga, Kvick & Abrahams, 1983). With Li located at $(0, 0, z)$, I at $(1/3, 2/3, 0)$ and O at (x, y, z) in space group $P6_3$, the temperature dependence of the O(z) coordinate is best described by the polynomial with zero first-order term as in

$$O(z)_T = -0.843\,5\,(3)\,\text{Å} + 62\,(4) \times 10^{-9} T^2\,\text{Å}\,K^{-2} \quad (5)$$

and that of Li by the comparable polynomial

$$Li(z)_T = 0.380\,8\,(10)\,\text{Å} + 167\,(18) \times 10^{-9} T^2\,\text{Å}\,K^{-2}. \quad (6)$$

Evaluation of these equations shows a displacement with respect to the invariant I atom, on heating through the interval 290–310 K, by the O atom of about 0.000 8 Å from (00.1) and by the Li atom of about 0.002 0 Å toward (00.1). Each displacement produces a positive polarization on (00.1), equivalent in orientation to the more steeply pointed end of crystals grown from aqueous solution at pH > 3 and the direction toward which the iodine apices of the IO_3^- ions point, in agreement with experimental observation (Abrahams, Liminga & Albertsson, 1990), see also § III.4. A value of $p_3' \simeq +34 \times 10^{-6}\,C\,m^{-2}\,K^{-1}$ may be calculated from (5) and (6) at room temperature, based on $\Delta P/\Delta T = e/V\sum qd$, where q is the charge on Li or that distributed over the three O atoms of the iodate ion, d is their displacement over a small temperature interval ΔT, and q is taken as unity. The temperature dependence of p_3 between 120 and 320 K (Bhalla, 1984) exhibits two maxima, rising to about $50 \times 10^{-6}\,C\,m^{-2}\,K^{-1}$ at 140 K and about $22 \times 10^{-6}\,C\,m^{-2}\,K^{-1}$ at 260 K with a room-temperature value of about $10^{-5}\,C\,m^{-2}\,K^{-1}$. The relatively small magnitude of p_3 and its departure from a monotonic thermal dependence, together with the monotonic atomic displacement dependence given by (5) and (6), suggest that p_3' and p_3'' may be comparable in magnitude but opposed in sign as previously suggested in Landolt-Börnstein (1984).

The thermal-expansion coefficients α_1 and α_3 of α-$LiIO_3$ between 20 and 520 K also vary monotonically (Abrahams, Liminga, Marsh, Schrey, Albertsson, Svensson & Kvick, 1983) but the piezoelectric stress coefficient magnitudes e_{31} and e_{33} are known only

close to room temperature. With the assumption of the same sign for e_{31} and e_{33}, the corresponding calculated value of p_3'' is 62×10^{-6} C m^{-2} K^{-1}; an assumption of opposite signs gives a magnitude of about 31×10^{-6} C m^{-2} K^{-1}, suggesting that the absolute sign of e_{31} is indeed negative. A negative e_{31} coefficient hence results in a net value of $p_3 = p_3' + p_3''$, which is not significantly different from observation. It may be noted that an erroneous report in the literature suggesting an opposite orientation sense for the piezoelectric d_{33} coefficient (e_{ij} and its corresponding d_{ij} coefficient have the same sign) to that given in § III.4 was caused by a failure to transform earlier Miller indices and atomic coordinates.

4. *Pyroelectric monoclinic lithium sulfate monohydrate*

$Li_2SO_4 \cdot H_2O$ numbers among the relatively few (31 are listed in Landolt-Börnstein, 1984) pyroelectric crystals for which both the total coefficient has been measured and the primary and secondary coefficients are also given: calculation of the latter has been provided in useful detail (Lang, 1971, 1974). The total pyroelectric coefficient p_2 was reported therein to vary over the range 4.2 to 310 K from about zero at the lowest temperature to a maximum negative value of about -8×10^{-6} C m^{-2} K^{-1} at about 60 K before returning to zero at 106 K and then rising to about 95×10^{-6} C m^{-2} K^{-1} at the highest measurement temperature. The value of p_2'' at 293 K, calculated from the piezoelectric, elastic stiffness and thermal-expansion coefficients, is 26×10^{-6} C m^{-2} K^{-1} with a resulting primary coefficient p_2' of about 69×10^{-6} C m^{-2} K^{-1} at room temperature: p_2' and p_2'' were found to have equal but opposite magnitudes at 106 K.

$Li_2SO_4 \cdot H_2O$ has space group $P2_1$ with $a = 5.455\,3\,(1)$, $b = 4.869\,0\,(1)$, $c = 8.176\,1\,(2)$ Å and $\beta = 107.337\,(2)°$ at 298 K (Karppinen, Liminga, Lundgren, Kvick & Abrahams, 1986). The structure has been determined at 20, 80 and 293 K by neutron diffraction (Lundgren, Kvick, Karppinen, Liminga & Abrahams, 1984) and at 80 and 298 K by X-ray diffraction (Karppinen *et al.*, 1986). Unlike the examples in §§ V.2 and V.3, $Li_2SO_4 \cdot H_2O$ is structurally multiparameter (29 variable atomic coordinates including the H atoms) with SO_4^{2-} ions and neutral H_2O molecules that are free to change orientation. Since the the majority of pyroelectrics contain ionic or molecular groups with a characteristic temperature-dependent contribution to the spontaneous polarization, this crystal presents a typical illustrative example of the relationship between pyroelectricity and structure.

The maximum observed structural changes between 20 and 80 K are only 0.006 (3) Å in an H···O bond length and 0.26 (10)° in an O–Li–O bond angle. The X-ray diffraction derived spontaneous polarization is hence considered only on the basis of the structures determined at 80 and 298 K (Karpinnen, Liminga, Kvick & Abrahams, 1988). The absolute polarity of a large crystal having been determined by the methods of § IV.5, the absolute d_{22} piezoelectric coefficient was found to be -16.3×10^{-12} C N^{-1} at 293 K, with an absolute p_2 pyroelectric coefficient $= -89.6 \times 10^{-6}$ C m^{-2} K^{-1} based upon Lang's (1971) magnitudes. The sign identity for d_{22} and p_2 shows that tensile stress and heating cause similar rotations in and displacements of the SO_4^{2-} and H_2O dipoles; either application also causes an expansion along the polar direction. The *IEEE Standard on Piezoelectricity* (1978) requires a choice of **b** in space group $P2_1$ that results in a positive value for d_{22}, hence both **b** and **c** axial vectors should be reversed in sign with comparable changes made in the y and z atomic coordinates for use in piezoelectric calculations.

Calculating the charge and dipole-moment distribution in the SO_4^{2-} ion and H_2O molecule on the basis of the net atomic charges determined from the experimental charge density (Karpinnen *et al.*, 1986) shows that the ion has a nonzero dipole moment of about 2.3×10^{-30} C m at 80 K that rotates through 9° in the *ac* plane between 80 and 298 K; similarly, the molecular dipole moment decreases from about 7.8×10^{-30} C m at 80 K to about 6.7×10^{-30} C m as it rotates by 3.6° in the *bc* plane. The total spontaneous polarization at 80 K may then be calculated as $4.4\,(5) \times 10^{-2}$ C m^{-2} and as $3.2\,(6) \times 10^{-2}$ C m^{-2} at 298 K along the positive direction of the polar axis, as given by Karpinnen *et al.* (1988). The calculated value of ΔP between 80 and 298 K is thus $-1.2\,(7) \times 10^{-2}$ C m^{-2}. The corresponding experimental magnitude of ΔP is 1.04×10^{-2} C m^{-2}, although its sign was lost in the original macroscopic measurement. Despite an agreement between measured and calculated ΔP magnitudes that is very satisfactory, the large combined standard deviation in the diffraction-derived value demonstrates the need for an accuracy with which average structure amplitudes are measured that is substantially higher than the combined standard uncertainty of about 1.2% for the X-ray and 2.0% for the neutron cases achieved in the studies cited.

5. *Pyroelectric atomic displacements*

The refined solution of a pyroelectric crystal structure at several temperatures provides, among much other information, the magnitude of each individual atomic displacement along the polar axis over the thermal interval between determinations. Relatively few nonferroelectric but pyroelectric crystals have been the subject of such a study. In the three examples of § V, the atomic polar displacement coefficient in ZnO for O with respect to Zn is $0.263\,(8) \times 10^{-4}$ Å K^{-1}; the polar coefficients in α-$LiIO_3$ for Li and O with respect

to I are nonlinear but, in the range 250–350K, may be approximated by 1.00 (10) and 0.37 (5) $\times 10^{-4}$ Å K^{-1}, respectively; in Li_2SO_4, the maximum polar coefficients for Li, O, H and O(water) with respect to S are 0.37 (9), 1.22 (5), 1.59 (6) and 2.86 (14) $\times 10^{-4}$ Å K^{-1}, respectively. The polar coefficients reported in other nonferroelectric pyroelectrics include 0.8×10^{-4} Å K^{-1} in α-$Cu(IO_3)_2$, 1.1×10^{-4} Å K^{-1} in $Nd(IO_3)_3 \cdot H_2O$, 1.1×10^{-4} Å K^{-1} in $3La(IO_3)_3 \cdot HIO_3 \cdot 7H_2O$, 0.3×10^{-4} Å K^{-1} in $LiClO_4 \cdot 3H_2O$, 0.2×10^{-4} Å K^{-1} in $Na(H_3O)[I(OH)_3O_3]$ and 1.5×10^{-4} Å K^{-1} in KIO_2F_2 (Abrahams, 1978).

It may be noted that all polar displacement coefficients (ξ) for measured nonferroelectric pyroelectrics lie in the range $3 > \xi > 0.2 \times 10^{-4}$ Å K^{-1}. The lower limit may be expected to approach zero as crystals with smaller pyroelectric coefficients are measured; the upper limit is unknown but is probably greatly exceeded by many ferroelectric pyroelectrics with magnitudes of p_i that exceed 10^{-3} C m^{-2} K^{-1}, see § VII.

6. *Structural information from absolute moduli*

Measurement of the absolute pyroelectric moduli over a wide thermal range provides a quantitative but independent basis for careful comparison with models derived from structure determination. Differences between macroscopic measurement and structural, *i.e.* microscopic, inferences provide the necessary guidance for improving the model. There is at present a paucity of absolute pyroelectric moduli measurement, but those comparisons that have been reported suggest an increasing difference between measured and calculated ΔP at lower temperatures that deserves further investigation, see for example § V.2.

7. *Future directions*

A pyroelectric crystal is best understood if its crystal structure is determined accurately at temperatures that sample its full stability range and if its absolute moduli are measured continuously over the same range. Both sets of measurement should be extended where possible to 5–10 K or lower. As electronic effects increasingly lead to differences between measurement and model such as those noted in the preceding section, it is apparent that the accuracy of the diffraction measurements must be improved substantially in order to yield an unambiguous pyroelectric model.

VI. Ferroelectricity

1. *Property description*

All pyroelectric crystals exhibit a polarization P_i along their polar i axis, see § IV.2. Crystals with a permanent electric dipole moment that is capable of being reoriented by the application of an external electric field are called ferroelectric, a term first introduced by analogy with ferromagnetism. The designations Seignette-electric and Rochelle-electric are no longer in use but are widely found in the earlier literature, in deference to the dielectric properties of the first ferroelectric crystal Rochelle salt, $NaKC_4H_4O_6 \cdot 4H_2O$, discovered by J. Valasek in 1921. All ferroelectric crystals are necessarily both pyroelectric and piezoelectric. The permanent polarization in most ferroelectric crystals disappears at a higher-temperature transition to another phase, usually referred to as the Curie temperature T_c. Ferroelectric crystals may undergo chemical decomposition, or may melt, at temperatures below T_c. A nonpolar phase above T_c is often designated the paraelectric phase although it may be antiferroelectric.

Ferroelectric crystals grown in the absence of an electric field are inevitably twinned and contain approximately equal domain volumes, each of which is characterized by a polarization oriented in a direction opposite to that of the other, thereby minimizing the crystal electrostatic energy. Electrically twinned crystals exhibit very small or zero macroscopic pyroelectric and piezoelectric effects. An early step in most investigations of the tensor properties of ferroelectric materials is hence crystal detwinning or poling, by the appropriate application of an electric field, to produce a single domain if the initial crystal is single. As in the case of pyroelectric crystals, a net macroscopic dipole is usually undetectable in aged ferroelectric crystals owing to the rapid formation of ambient neutralizing charges on the crystal surfaces. The properties of polycrystalline ferroelectrics, although important technologically for their associated attributes (see Burfoot & Taylor, 1979, for example), are not considered below.

Ferroelectricity was generally thought of as a highly anomalous property in the years following its discovery. The second crystal with ferroelectric properties, KH_2PO_4 (KDP), was not recognized until 1935 and provided apparent confirmation for the view that ferroelectricity was directly related to hydrogen bonding. A series of ferroelectrics isomorphous with KDP was discovered in Zürich in the following years that tended to reinforce this belief. Widespread interest in ferroelectricity began only with the discovery in 1944 of a third group of ferroelectric materials, typified by $BaTiO_3$ with its rather rectangular polarization hysteresis loops. The high dielectric permittivities of ferroelectric crystals with their reversible polarizations and their superior optoelectronic properties led thereafter to a search for new candidate materials, with a resulting steady discovery rate of about four to five new single-component ferroelectrics annually that still continues.

2. *Spontaneous polarization*

Several methods are in common use for measuring the magnitude of the permanent spontaneous polarization

P_s of a ferroelectric crystal, including hysteresis loop, charge integration, polarity reversal and calibrated pyroelectric techniques (see *e.g.* Lines & Glass, 1977). The magnitude of P_s in single-domain ferroelectric crystals usually lies within the range 10^{-4} to $1\,C\,m^{-2}$ and may have a nonzero value only in the ten crystal classes for which pyroelectricity is allowed, see § IV.4. The thermal dependence of P_s for small values of ΔT is equivalent to the pyroelectric coefficient p_i at that temperature. P_s shares an origin in common with the polarization producing p_i, primarily the sum of the individual point electric dipoles distributed throughout the unit cell. Unlike the polarization in the majority of pyroelectric crystals, however, P_s has the unique characteristic of being reversible or, in some symmetry-allowed cases, reorientable.

3. *Dielectric hysteresis*

The application of a d.c. field E greater than the coercive field E_c along the polar direction of a polydomain ferroelectric single crystal causes reorientation of the antiparallel P_s vectors present in about half the total number of domains, leading to an orientation in which all P_s vectors assume a parallel state. The reorientation involves the motion of the domain walls separating regions with parallel P_s from those with antiparallel (*i.e.* $-P_s$) vectors, followed by the growth of domains with parallel P_s vectors as the domain walls are gradually swept out of the crystal as E increases. The minimum d.c. field needed to move the domain walls is a measure of the coercive field, see Fig. 4. Initial application of a d.c. field less than coercive to a polydomain crystal will not change the initial effectively zero value of the macroscopic crystal polarization. As the d.c. field strength approaches that of the coercive field at a given temperature, the effective polarization starts slowly to increase, thereafter increasing rapidly to a maximum saturated value of P_s.

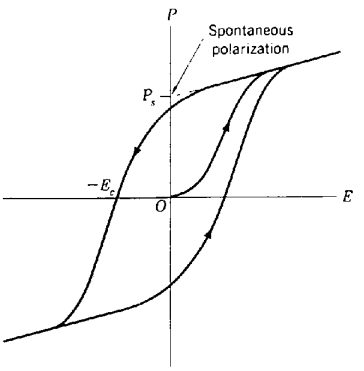

Fig. 4. Ferroelectric hysteresis loop, illustrating the effect of applying a d.c. field E along the polar axis of an as-grown ferroelectric crystal. The resulting polarization P is initially zero, reaching saturation at large E. Spontaneous polarization P_s and coercive force E_c are shown (after Kittel, 1971).

The single domain crystal thereby produced is generally stable in the absense of the applied field, although it is possible for a limited reverse nucleation to occur with a resulting remanent polarization less than the full P_s. This effect may be caused by residual stresses in the crystal or by nonequilibrated free charges at the crystal surfaces. If the applied d.c. field at the saturated value of P_s is decreased, the polarization will start to decrease as domain walls enter the crystal to form domains of antiparallel orientation. On reaching zero applied field, more P_i vectors will remain parallel than antiparallel thereby resulting in a remanent P_r polarization. Increasing the strength of the reversed d.c. field continues to decrease the macroscopic polarization until it becomes zero as a balance is reached between the parallel and antiparallel P_i vectors. Further increase in the reversed field strength leads finally to all P_i vectors occupying the antiparallel state, giving a saturated value of $-P_s$. A full hysteresis loop is formed by reducing the reversed field to zero, then gradually increasing until $+P_s$ is again reached, see Fig. 4. In the event that $P_r = P_s$, the resulting hysteresis loop is rectangular, generally an advantage in rapid switching of polarization states.

As-grown unpoled ferroelectric crystals characteristically contain a domain pattern that is generally easy to observe between crossed polarizers owing to their birefringence. Viewed along the polar direction of a uniaxial crystal, the material appears dark as the crystal is rotated about this direction but is bright along all other directions. The domains in optically biaxial crystals are birefringent for all orientations, hence readily observable. The boundary between two domains is the domain wall. Poling the crystal to remove all domain walls yields the full P_s and eliminates the domain pattern. Several other techniques commonly used to reveal domain patterns have been described by Lines & Glass (1977), see also *International Tables for Crystallography* (1994).

4. *Absolute sense of spontaneous polarization*

The absolute sense of P_s with respect to the atomic arrangement may be determined with confidence following the reliable refinement of a given ferroelectric crystal structure. The requirements for the latter are often more stringent than for other crystal structure determinations, and include full characterization of the physical properties of the crystal from which the diffraction sample is taken, the use of a single domain sample, confirmation of the point group by physical measurement before initiating the structure determination, and accurate measurement of the structure amplitudes and their uncertainties. Failure to meet all four conditions can lead to unexpected difficulties with the subsequent interpretation of the diffraction results. Many ferroelectrics either melt incongruently, with a resulting defect structure that can cause significant variation in properties (see $LiNbO_3$ for example, § VII.3), or have a variable composition for

other reasons (*e.g.* $Ba_2NaNb_5O_{15}$ with a Curie temperature, lattice parameters, refractive index *etc.* that vary both with Ba/Na ratio and heat treatment).

An unambiguous relationship between structure and property clearly depends on a material commonality between them. A single-domain sample is necessary for X-ray diffraction measurements in the ferroelectric phase if the small displacements of atoms from their higher-temperature symmetry positions are to be resolved successfully from comparable or larger-amplitude thermal displacements. Not only does this resolution decrease as the ratio of domains of opposite sense decreases, but the difficulty of distinguishing the polar from the equivalent centrosymmetric point group increases; it is always preferable to determine the actual point group on the basis of a clear physical measurement (*cf.* Recommendation 7 of Schwarzenbach *et al.*, 1989). It has been estimated that the average uncertainty of each structure amplitude measured in a typical inorganic ferroelectric [*i.e.* $u_c(F^2_{obs})/F^2_{obs}$, where $u_c(F^2_{obs})$ is the combined standard uncertainty in F^2_{obs}, see *ISO Guide to the Expression of Uncertainty in Measurement* (1993)]* should be no greater than about 1% and preferably smaller than about 0.5% to provide the basis for a satisfactory structure–ferroelectric property relationship.

Once the relationship between atomic arrangement and the polar-axis sense has been determined, two further experiments that are performed on the same crystal are necessary in order to determine the absolute sense of P_s and hence the absolute ferroelectric structure. In the first experiment, the sense of P_s is measured relative to the crystal orientation, then the absolute atomic arrangement is determined for this orientation by means of an X-ray dispersion measurement (see § II.5); the combination of these results gives the absolute sense of P_s.

VII. Structure and ferroelectricity

1. *Atomic displacement and* T_c

The crystal structures of all known inorganic ferroelectrics may be characterized by displacement vectors Δz along the polar direction for one or more cations or atoms within the unit cell from a higher-symmetry position, with respect to the sublattice formed by the anions, which may exhibit a more or less distorted arrangement, see below. The vector $2\Delta z$ connects the displacement for each atom corresponding to a given sense of P_s to the symmetry-related displacement for the same atom in an orientation with P_s of opposite sense. The displacement vector vanishes at the phase transition T_c if the higher-temperature phase is paraelectric; commonly, the sublattice distortion also decreases above T_c. The relationship in (7) between the displacement Δz and T_c was initially found by Abrahams, Kurtz & Jamieson (1968) to fit the values of these parameters in a group of 12 oxygen-framework ferroelectrics:

$$T_c = (\mathcal{K}/2k)(\Delta z)^2\,\mathrm{K}, \qquad (7)$$

where $\mathcal{K}$ is a force constant, k is Boltzmann's constant, Δz is the largest displacement component along the polar direction from the zero spontaneous polarization position occupied by the metal atom forming the shortest and least-ionic bonds in the structure and $\mathcal{K}/2k \simeq 2.00\,(9) \times 10^4\,\mathrm{K\,\AA^{-2}}$; (7) has been shown in many subsequent studies to apply rather generally, although $\mathcal{K}$ is expected to be structure dependent.

Five illustrative ferroelectrics to which (7) has been applied are considered below. The first is $BaTiO_3$, which is also the first non-hydrogen-bonded ferroelectric to be discovered and in addition is one of the most intensively investigated of all inorganic materials. The structure of $BaTiO_3$, which is based upon corner-connected TiO_6 octahedra and which is also ferroelastic at room temperature, is not only important on its own merits but it also presents a valuable warning by typifying a major difficulty associated with ferroelectric crystal-structure determination. The second, $LiNbO_3$, is also based upon a framework of oxygen-octahedra building blocks; this material is widely used in a range of technological devices and illustrates well the effects of nonstoichiometry upon structure-dependent properties. The third is $Tb_2(MoO_4)_3$; the isolated tetrahedra in this material and the expected change in force constant $\mathcal{K}$ led to its structural study as a function of temperature through T_c. Like $BaTiO_3$, $Tb_2(MoO_4)_3$ is also a ferroelectric–ferroelastic but in this case the two properties are coupled, see § VIII.6. The two final examples, taken from the recently enlarged field of fluoride ferroelectrics, are the coupled ferroelectric–ferroelastic $K_3Fe_5F_{15}$ and the recently discovered ferroelectric family typified by $Pb_5Al_3F_{19}$ with its multiphase transition behavior.

2. *Ferroelectric–ferroelastic tetragonal barium titanate*, $BaTiO_3$

The first ferroelectric discovered that did not involve a hydrogen bond, this oxygen-framework perovskite structure opened the modern field of polar dielectrics in 1944; ferroelectricity had previously been considered an anomalous dielectric behavior dependent upon an unspecified characteristic of the hydrogen bond. Many other ABO_3 materials with similar structure followed the discovery of $BaTiO_3$; numerous complex perovskitic structure oxides with formula $A_xA'_{1-x}B_yB'_{1-y}O_3$ have subsequently been shown to be ferroelectric and a compilation of materials with a tabulation of all relevant

* The report by the IUCr Working Group on the Expression of Uncertainty in Measurement is at present being reviewed for publication in *Acta Cryst. Section A.*

properties is conveniently given in Landolt-Börnstein (1981). More than 11 independent structural studies have been published on tetragonal $BaTiO_3$ since 1947, including the use of temperature and pressure as variables in the investigations.

Pure $BaTiO_3$ has a Curie temperature of 403 K with $a = 3.992\,0$, $c = 4.036\,1$ Å and space group $P4mm$ at 293 K (Landolt-Börnstein, 1981); the corresponding atomic displacement Δz of Ti, with respect to the center of its oxygen octahedron, is 0.142 Å as calculated from (7). It may be noted that, for Ba at the polar origin, the only structural variables are z(Ti), z(O1) and z(O2), which are respectively close to the values $\frac{1}{2}$, 0 and $\frac{1}{2}$ below T_c and which assume these special values at and above T_c; all recent studies agree that z(Ti) is displaced from its special value in the opposite sense to the displacements of O1 and O2. The magnitude of Δz as defined for use in (7) is the displacement of Ti from the center of its distorted octahedron and is given by the expression $[2z(\mathrm{O1}) + 4z(\mathrm{O2}) - 2]/6$. The earlier quantitative X-ray diffraction investigations, exemplified by Evans (1961), reported gross matrix vector interactions between the z coordinates of the Ti or O atoms and the corresponding U_{33} atomic displacement parameters, with a resulting indeterminacy in each pair of parameters. The combined neutron and X-ray diffraction study of Harada, Pedersen & Barnea (1970) overcame the indeterminacy by assuming all U_{33} to be approximately equal and reported $\Delta z(\mathrm{Ti}) = 0.128\,(3)$ Å; however, they noted a residual correlation of 98% between z(Ti) and U_{33}(Ti). Two X-ray diffraction sets of higher precision were used in the most recent study (Buttner & Maslen, 1992), neither of which eliminated the major correlation between z(Ti) and U_{33}(Ti), to give $\Delta z(\mathrm{Ti}) = 0.134\,(23)$ and $0.112\,(77)$ Å. The values of Δz(Ti) from the two sets agree with that predicted above using T_c and (7), but with insufficient accuracy to draw further structural conclusions.

It is noted that all crystals used in the diffraction studies of $BaTiO_3$ were as-grown, *i.e.* unpoled, and hence may be expected to contain equal numbers of ferroelectric domains of opposite polarity. The diffraction experiment, which samples each unit cell throughout the crystal, is hence unable to distinguish between the scattering from the actual ferroelectric atomic array and one with a unit cell in which the atom at each site has a displacement of about 0.1 Å both parallel and antiparallel to the polar direction. A high correlation between Δz and U_{33} for both Ti and the two independent O atoms, if the displacements of both variables for each atom are of comparable dimension, is thus inevitable for unpoled samples.

Tetragonal $BaTiO_3$, with $a \simeq c$ and atomic coordinate relationships $x_1\, y_1\, z_1 = x_2\, z_2\, y_2 + \Delta$ or $x_1\, y_1\, z_1 = z_2\, y_2\, x_2 + \Delta$, where $\Delta < 0.08$ Å, is hence also structurally ferroelastic with $e_{32} = 5.49 \times 10^{-3}$, see § IX.1. Compressive stress applied along the polar direction is predicted to rotate this axis through 90°; the given pair of coordinate relationships leads to the further prediction that such an application along the c direction is likely to result in an approximately equal distribution of the polar axis along both former a axes. Rotation of **c** only to the a_2 direction requires that the application of compressive stress is confined to the (010) plane, preferably closely along [101]. Despite the ferroelastic and ferroelectric properties in $BaTiO_3$ being partially coupled, the polar sense is not conserved on axial reorientation. Ferroelectric, ferroelastic reorientation in a poled crystal is hence bound to result in an unpoled crystal.

3. *Ferroelectric trigonal lithium niobate*

Recognition of the value of $LiNbO_3$ as an electrooptic material with switching speeds in excess of 50 ps has led to its widespread use in such devices as modulators, high-speed switches, waveguide arrays, multiplexers, filters, surface acoustic wave devices and polarization converters. Although the material with its related desirable properties was found to be ferroelectric within about five years of discovering $BaTiO_3$, the development of these properties was delayed until the Czochralski technique had been exploited to grow large single-crystal boules (Nassau, Levinstein & Loiacono, 1966). Earlier diffraction studies by Bailey (1952; quoted by Megaw, 1952) on an unpoled crystal and by Shiozaki & Mitsui (1963) on a polycrystalline sample gave ambiguous structural results, but accurate measurements with an automatic diffractometer on a single-domain sphere of $LiNbO_3$ led to a reliable structure determination (Abrahams, Reddy & Bernstein, 1966). A pair of simplified views of the structure [$a = 5.147\,39\,(8)$, $c = 13.856\,14\,(9)$ Å at 298 K in space group $R3c$], shown in Fig. 5, suggests the atomic displacements undergone in reversing the sense of P_s through a paraelectric state with $P_s = 0$ (Fig. 5*c*); the Nb atom moves a total $2\Delta z$ from $-\Delta z$ below the center of its octahedron (Fig. 5*b*) along **c** to $+\Delta z$ above the center (Fig. 5*d*) as the Li atom passes through its nearest shared (triangular) octahedral face (see Figs. 5*a*, *c*) in the same direction as Nb to the corresponding position above that face (or *vice versa*). The Nb-atom displacement derived from this diffraction study is $\Delta z = 0.269$ Å; that predicted by means of (7) from the best 1966 value of $T_c = 1483$ K is 0.272 Å.

A recent structural re-examination of $LiNbO_3$ (Abrahams & Marsh, 1986) illustrates the major influence that departures from stioichiometry can have on relationships between 'structure' and properties. Crystal samples for diffraction analysis, particularly if taken from large optical-quality boules of a given material, are commonly regarded as fully representative of the material; the latter assumption is frequently made under less well defined crystal-growth conditions. Failure to

consider the effects that nonstoichiometry may have on a ferroelectric crystal-structure determination can lead to incorrect inferences being drawn. $LiNbO_3$, as in the case of many other mixed oxides, melts incongruently. In consequence, crystals grown from a melt with a composition other than congruent exhibit a range of departure from stoichiometry. Among the properties known to vary with composition in $LiNbO_3$ are the Curie temperature T_c (by over 70 K), the refractive index n_e (of critical concern in the performance of electrooptic switches), the density, the isotopic distribution (variations of ^6Li concentration in starting materials affect the final Li concentration in the grown boules), the in-diffusivity of other metals (used in producing waveguides on single-crystal plates of $LiNbO_3$) and the lattice parameters (see *Properties of Lithium Niobate*, 1989). Congruently grown crystals, and others with Li-deficient compositions, can be converted into stoichiometric $LiNbO_3$ by exposure to Li vapor at a temperature close to T_c. Full characterization of a given crystal sample is essential for significant correlation of measured properties with those measured on other samples.

The 1986 structural study finds $\Delta z = 0.276\,8\,(7)$ Å in stoichiometric and $0.270\,1\,(7)$ Å in congruent $LiNbO_3$ with $T_c = 1532$ and 1459 K, respectively, as predicted by (7). The experimental values are 1471 and 1402 K. The 1986 study noted that reduction of the average force-constant-to-Boltzmann-constant ratio from 2.00×10^4 in (7) to 1.93×10^4 K Å^{-2}, corresponding to a force-constant change from 55.2 to 53.3 J m^{-2} results, respectively, in the predicted T_c values of 1477 and 1408 K. In stoichiometric material, the Li site is found to be 100% occupied by Li, the Nb site by 100% Nb and the O site similarly 100% occupied by O, as expected; in congruent material, with the composition $Li_2O{:}Nb_2O_5 = 48.45{:}51.55$, the Li site is found to contain 94.1 (3)% Li and 5.9 (3)% Nb while the Nb site contains 95.3 (3)% Nb and 4.7% vacancies for 100% assumed occupation by oxygen of the O sites. The defect structure in nonstoichiometric lithium nobate may be represented by the chemical formula $[Li_{1-5x}Nb_{5x}]Nb_{1-4x}O_3$, with a total stable phase field given by $0 \leq x \leq 0.02$, where the Li-site occupancy is provided within square brackets.

It is hence highly advisable to precede all structure determinations of ferroelectric crystals by undertaking preliminary density and lattice-parameter measurements that are accurate enough to detect significant departures from the nominal stoichiometry and, if found, to include this information in the refinement model; it is also most prudent to reduce later possible structural ambiguities by using a poled single-domain crystal sample for the intensity measurements.

4. *Ferroelectric–ferroelastic terbium molybdate*

β-$Tb_2(MoO_4)_3$ is a fully coupled ferroelectric–ferroelastic crystal with $T_c = 436$ K, $P_s = 0.19\,(1) \times 10^{-2}$ C m^{-2} and $e_{12} = 2.016 \times 10^{-3}$ at 298 K (Keve, Abrahams, Nassau & Glass, 1970) with $a = 10.344\,43\,(5)$, $b = 10.386\,23\,(5)$ and $c = 10.654\,85\,(4)$ Å in space group $Pba2$. The structure was determined at 298 K using a single-domain crystal (Svensson, Abrahams & Bernstein, 1979). The coupling of ferroic properties is completely structure dependent, as shown by (8), since each atom at (x_1, y_1, z_1) in β-$Tb_2(MoO_4)_3$ at 298 K is related to another atom of

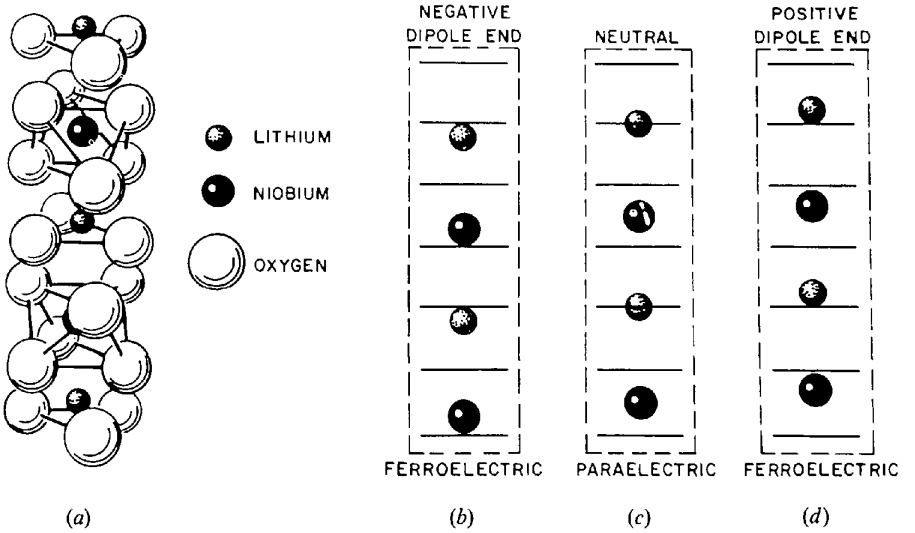

Fig. 5. Ferroelectric $LiNbO_3$ structure with (*a*) the sequence of distorted O-atom octahedra containing an Nb atom, a vacancy and an Li atom, respectively, along the polar axis, (*b*) schematic of (*a*) with O-atom sheets represented by line segments and Li and Nb atoms shown between sheets, (*c*) schematic with Nb atom at inversion center and Li atom on mirror, and (*d*) as in (*b*) but with opposite polarity (after Abrahams & Keve, 1971).

the same kind at (x_2, y_2, z_2):

$$(x_1, y_1, z_1) = \left(\tfrac{1}{2} - y_2, x_2, 1 - z_2\right) + \Delta, \qquad (8)$$

where Δ is a displacement vector joining the pairs of (x_1, y_1, z_1) and (x_2, y_2, z_2) coordinates and is found to be uniformly less than 0.7 Å in length for all 17 independent atom pairs. It may be inferred from (8) and the lattice-parameter magnitudes that a compressive stress applied along [010] will reorient the unit cell such that the **a** and **b** axial vectors transform to $-\mathbf{b}$ and **a**, respectively, as the sense of the polar c axis is reversed. The stress may be either an electric field applied along **c**, a tensile stress applied along the shorter a, or a compressive stress applied along the longer b axis. A view of the structure in both ferroelectric–ferroelastic orientations is shown in Fig. 6.

The structure of $Tb_2(MoO_4)_3$ was also measured at 373, 438, 463 and 523 K in order to follow the temperature dependence of the atomic positions through the second-order phase transition at T_c to tetragonal space group $C\bar{4}m2_1$ (Abrahams, Svensson & Bernstein, 1980). The MoO_4^{2-} tetrahedra rotate smoothly with temperature about their internal axes by less than 8° between 298 and 438 K (taking the latter as approximately equal to T_c), in contrast to the rotations of the comparable SO_4^{2-} tetrahedra in piezoelectric $K_2Cd_2(SO_4)_3$. In the latter first-order phase transition, over 70% of the angular rotations take place within a few degrees of T_c (Lissalde, Abrahams, Bernstein & Nassau, 1979), whereas in β-$Tb_2(MoO_4)_3$ the rotational variation is proportional to P_s and e_{12} over the experimental thermal regime.

The force constant characterizing the displacement of metal atoms from their octahedral centers in ferroelectric crystals, for the case of slightly distorted cubic or hexagonal close-packed O-atom frameworks typified by $BaTiO_3$ and $LiNbO_3$, is expected to differ significantly from that in materials such as β-$Tb_2(MoO_4)_3$. In the latter case, each tetrahedron is free to rotate or undergo displacement as an isolated ion; in addition, the tetrahedral dipole may change as the metal atom becomes displaced from the center of its tetrahedron or the tetrahedral distortion changes. It may also be noted that β-$Tb_2(MoO_4)_3$ is a representative of the three-dimensional ferroelectric class (Abrahams & Keve, 1971) in which polarity reversal or reorientation involves similar-magnitude displacements along all three axial directions, with a consequent spontaneous polarization that typically is less than about 3×10^{-2} C m^{-2}, whereas P_s in $BaTiO_3$ and $LiNbO_3$ is an order of magnitude or more greater. The largest ferroelectric displacements along the polar direction by the metal atoms from the centrosymmetric positions in β-$Tb_2(MoO_4)_3$ at room temperature are less than 0.01 Å, with the largest Mo displacements including all x, y and z components less than 0.1 Å. The value of P_s may be calculated from the structure by means of (3) as 0.09×10^{-2} C m^{-2}, assuming the Tb^{3+} charges are located at the Tb- and the $(MoO_4)^{2-}$ charges at the Mo-atom positions; agreement between experimental (see above) and calculated P_s magnitudes is rarely better in three-dimensional ferroelectrics.

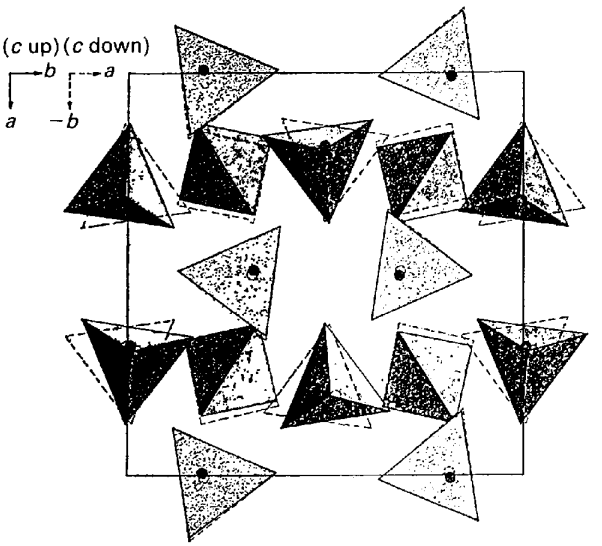

Fig. 6. Arrangement of Tb^{3+} (circles) and $(MoO_4)^{2-}$ ions in ferroelectric–ferroelastic β-$Tb_2(MoO_4)_3$ at 298 K. Solid outlines represent atomic positions in a cell with orientation **a b c**, dashed outlines in a reoriented cell with orientation $-\mathbf{b}$ **a** $-\mathbf{c}$. Application of a stress along [010] or an electric field along [001], each of which exceeds the coercive force, results in switching from one orientation to the other (after Svensson, Abrahams & Bernstein, 1979).

5. *Ferroelectric–ferroelastic* $K_3Fe_5F_{15}$

Among the more recently discovered new ferroelectric materials, $K_3Fe_5F_{15}$ was first predicted to be a coupled ferroelectric–ferroelastic (Abrahams, 1989) on the basis of the previously published crystal structure (Hardy, Hardy & Ferey, 1973). For each atom in the unit cell at (x_1, y_1, z_1) there is a like atom at (x_2, y_2, z_2) such that

$$(x_1, y_1, z_1) = \left(\tfrac{1}{2} - y_2, \tfrac{1}{2} + x_2, -z_2\right) + 2\Delta \qquad (9)$$

with a maximum value of $\Delta < 0.32$ Å, where 2Δ is the connecting vector between corresponding pairs of atoms at these two locations. Equation (9) shows that, as the a axis exchanges identity with the b axis (axis exchange is the characteristic of ferroelasticity) and *vice versa*, the polar c axis also reverses sense (the characteristic of ferroelectricity) in the unit-cell transformation **a**, **b**, **c** = $-\mathbf{b}$, **a**, $-\mathbf{c} + \Delta'$, where Δ' is the mismatch unit-cell vector between the two orientations. Taking the Fe–F bonds as the strongest and least ionic in $K_3Fe_5F_{15}$, with $a = 12.750$, $b = 12.637$, $c = 3.986$ Å and space group $Pba2$ at room temperature, T_c was predicted to be 535 K based on (7) and the largest displacement by an Fe atom

from the paraelectric mirror plane of 0.163 Å. It may be noted that $K_3Fe_5F_{15}$ has a deformed tetragonal tungsten bronze structure, and hence consists of a close-packed array of F atoms with the K and Fe atoms occupying the interstices.

Optical microscopy reveals a characteristic 90° ferroelastic domain pattern in as-grown crystals that disappears sharply above 490 (10) K, calorimetry shows a λ-type heat-capacity anomaly at 490 (10) K, and the dielectric permittivity exhibits a sharp maximum at 495 (10) K at low frequencies that gradually dissipates at higher frequencies with a dispersion of about 10 K between 10^2 and 10^4 Hz, characteristic of relaxor ferroelectrics (Ravez, Abrahams & de Pape, 1989). $K_3Fe_5F_{15}$ is the first known fluoride to crystallize in a distorted tetragonal tungsten bronze structure with all the ferroelectric and ferroelastic attributes of this family. Further examination of the published orthorhombic atomic arrangement led to the prediction by Ravez *et al.* (1989) that below T_c the mixed valence Fe^{2+} and Fe^{3+} ions were ordered whereas above T_c the two kinds of ion were disordered. Mössbauer spectroscopy measurements (Calage, Abrahams, Ravez & de Pape, 1990) confirmed the prediction with the thermal dependence of both Fe^{3+} quadrupolar splitting and Fe^{3+} isomer shift, as well as the average Fe^{2+} quadrupolar splitting, undergoing a sharp and reproducible change in slope at T_c. The proportion of Fe^{2+} present below T_c is close to the stoichiometric 60% value, decreasing rapidly above T_c to less than 50% by 543 K, consistent with increasing delocalization of an Fe^{2+} electron.

6. *Ferroelectric* $Pb_5Al_3F_{19}$ *family*

Following the structural prediction and experimental verification of ferroelectricity in $SrAlF_5$ (Abrahams, Ravez, Simon & Chaminade, 1981) and $Sr_3(FeF_6)_2$ (Abrahams, Ravez, Canouet, Grannec & Loiacono, 1984), a study of the binary system AF_2–MF_3, with A = Sr, Ba and M = Ti, V, Cr, Fe, Ga, led to a series of new ferroelectric materials with formula $A_5M_3F_{19}$ and a structure isomorphous with that of ferroelectric $Pb_5W_3O_9F_{10}$ (Ravez, Arquis, Grannec, Simon & Abrahams, 1987). This series was later extended to include A = Pb and M = Al, Ti, V, Cr, Fe, Ga (Ravez, Andriamampianina, Simon, Grannec & Abrahams, 1991). $Pb_5Al_3F_{19}$, which forms four distinct phases including all those known among the other members of the family, may be regarded as the family prototype (Ravez, Andriamampianina, Simon, Rabardel, Ihringer & Abrahams, 1994). Ferroelectric $Pb_5Al_3F_{19}$ phase IV, formed on cooling phase III below 110 K, is isomorphous with $Pb_5Cr_3F_{19}$ phase II at 295 K in space group *I4cm* with a = 14.384 and c = 7.408 Å. The structure of $Pb_5Al_3F_{19}$ phase IV consists of corner-connected chains of AlF_6 octahedra and isolated octahedra; the close-packed F atoms form tricapped trigonal prisms and bisdisphenoidal polyhedra occupied by Pb. All atoms in $Pb_5Cr_3F_{19}$ phase II lie within 0.72 Å of a centrosymmetric arrangement, with a largest displacement Δz = 0.189 Å along the polar direction by a Cr atom from the center of its octahedron (Abrahams, Albertsson, Svensson & Ravez, 1990). Substitution of this Δz value in (7) gives T_c = 635 K; the experimental value is 555 K (Arquis-Canouet, Ravez & Abrahams, 1986).

The transition from antiferroelectric $Pb_5Al_3F_{19}$ phase III in space group *P4/n* to ferroelectric phase IV in space group *I4cm* is associated with a structural change from an eclipsed arrangement of AlF_6 octahedra along the inversion and rotation-tetrad axes in the former to a staggered arrangement of octahedra along the rotation-tetrad axes in the latter (Andriamampianina, Gravereau, Ravez & Abrahams, 1994). It may be noted that the barrier to the resulting octahedral rotations of ~45° at the T_c phase transition leads to an unusually large thermal hysteresis of about 170 K in the transition temperature as observed between heating and cooling, in addition to a wide and stable thermal regime over which the two phases coexist.

7. *Property prediction and polarization reversal atomic displacements*

The relationship between structure and ferroelectricity is now understood well enough that a crystal with previously unrecognized ferroelectric properties and for which the atomic coordinates have been carefully determined may be used as the basis for a structural deduction of the presence of that property. The structural criteria (Abrahams, 1988) upon which the prediction of ferroelectricity in such a crystal rests are: (*a*) the crystal must be polar; (*b*) the maximum displacement of no atom within the unit cell from its location corresponding to zero P_s must be greater than about 1 Å along the polar direction; and (*c*) the largest atomic displacements from the zero P_s positions must be significantly greater either than ~0.1 Å or the r.m.s. amplitude of thermal displacement for that atom.

The above criteria have been applied systematically to the atomic coordinates of all inorganic structures listed in the Inorganic Crystal Structure Database (see *Crystallographic Databases*, 1987) in several point groups. A sample of the predicted ferroelectric materials has been prepared and each one made has been experimentally verified as having ferroelectric properties. The criteria are currently in the process of being applied to additional point groups. A major source of new ferroelectrics would become available if all new crystal-structure determinations that are found to satisfy the three criteria above were tested experimentally for ferroelectric behavior by the structural investigator.

The nature of the structural changes resulting from the reversal of P_s by an electric field has been discussed for many ferroelectrics. Direct observation of

the corresponding atomic displacements has not yet been made. The techniques outlined in § III.8, using high-intensity synchrotron radiation and a detector that is gated to a preset level of the applied d.c. field, should in principle provide diffraction-intensity information sufficient to follow the motion of each atom as a function of field and temperature. In the case of $LiNbO_3$, for example, polarization reversal implies the motion of Li^+ ions through the triangular face of O atoms separating filled from empty octahedra as the Nb atom similarly moves along the polar axis from one side of its octahedral center to the other, see Fig. 5. The effect of the Li^+ ion on the O atoms as it approaches closer is presently unknown but is of considerable interest since, in isomorphous $LiTaO_3$, this ion is found to become disordered at 940 K with equal occupancy of a position 0.37 (2) Å from either side of the triangular face above the $T_c = 907$ K transition (Abrahams, Buehler, Hamilton & LaPlaca, 1973). Experiments of this kind will give not only an increased understanding of the polarization reversal mechanism but also a sensitive probe of the interaction between adjacent atoms as they are brought closer together.

VIII. Ferroelasticity

1. *Property description*

Ferroelasticity was first recognized as a new property by Aizu (1969), although its effects in the form of mechanical twinning and lattice reorientation in response to an applied mechanical stress were already well known, see *e.g.* Klassen-Neklyudova (1964). Many crystals are demonstrably ferroelastic, and the first surveys with a structural basis appeared soon after Aizu's paper (Abrahams & Keve, 1971; Abrahams, 1971): a recent survey appears in a book edited by Salje (1990). Ferroelasticity may be present in a material either as an independent property or coupled to another property, such as ferroelectricity; a variety of effects follow as crystal axes are interchanged under the application of mechanical stress, such as sharp changes in optical propagation or in macroscopic dimensions. If the ferroelastic property is coupled with another property, then axial interchange may be realized either by the application of a sufficiently large stress or a field able to reorient the second (coupled) property. Devices based upon a coupled ferroelastic–optic effect, for example, include modulators, displays, memories and pattern generators.

2. *Spontaneous strain*

A crystal is said to be ferroelastic if it contains two or more equally stable orientational states, in the absence of mechanical stress, and if the application of stress along an appropriate direction reproducibly transforms one such state into another (a condition often referred to as 'ferroelastic switching') . Ferroelasticity is always associated with a small distortion from a higher-symmetry state that may be only hypothetically stable. The spontaneous strain e_s is a measure of this distortion,† with magnitude typically on the order of or less than 10^{-3}. The minimum stress required for ferroelastic switching is the coercive stress E_{ij}, where i, j, respectively, denote the stress and transformed axis directions. The experimental magnitude of E_{ij} is a function of temperature, pressure and crystal defect distribution; the common range is $10^4 < E_{ij} < 10^8$ N m^{-2}. It may be noted that moderate finger pressure on a 1 mm^2 area produces a stress on the order of 10^6 N m^{-2}, *cf.* § III.6.

The spontaneous strain e_s is a second-rank tensor, hence the component magnitudes are not uniquely definable because of their dependence on the setting of the two unit cells although they may be determined from the measured lattice parameters. A good discussion on the tensorial aspects of physical properties is given in *International Tables for Crystallography* (1994). Following Salje (1990), the general triclinic case with lattice parameters given by $a, b, c, \alpha, \beta, \gamma$ in the low-symmetry phase and by $a_o, b_o, c_o, \alpha_o, \beta_o, \gamma_o$ in the high-symmetry phase have a spontaneous strain for the case with b-axis direction common to both phases and the z direction in the strain tensor Cartesian system parallel to $\mathbf{c}^*$:

$$
\begin{aligned}
e_{11} &= (a \sin\gamma / a_o \sin\gamma_o) - 1, \\
e_{22} &= (b/b_o) - 1, \\
e_{33} &= (c \sin\alpha \sin\beta^*)/(c_o \sin\alpha_o \sin\beta_o^*) - 1, \\
e_{23} &= \tfrac{1}{2}\{(c\cos\alpha)/(c_o \sin\alpha_o \sin\beta_o^*) \\
&\quad + [(\cos\beta_o^*)/(\sin\beta_o^* \sin\gamma_o)] \\
&\quad \times [(a\cos\gamma)/a_o - (b\cos\gamma_o)/b_o] \\
&\quad - (b\cos\alpha_o)/(b_o \sin\alpha_o \sin\beta_o^*)\}, \\
e_{13} &= \tfrac{1}{2}[(a \sin\gamma \cos\beta_o^*)/(a_o \sin\gamma_o \sin\beta_o^*) \\
&\quad - (c \sin\alpha \cos\beta^*)/(c_o \sin\alpha_o \sin\beta_o^*)], \\
e_{12} &= \tfrac{1}{2}[(a\cos\gamma)/(a\sin\gamma_o) - (b\cos\gamma_o)/(b_o \sin\gamma_o)],
\end{aligned}
\tag{10}
$$

where values with asterisks indicate reciprocal-lattice parameters and the standard tensor notation e_{ij} is used. The formulas in (10) apply also to higher-symmetry systems, with symmetry-forbidden components taking zero value. The magnitude of e_s is often taken as $\left(\sum e_{ij}\right)^{1/2}$, where the e_{ij} are as defined in (10).

Spontaneous strain magnitudes for 20 different materials, gathered by Salje (1990) from the literature, range

† Although e_{ij} is the accepted symbol for the piezoelectric stress coefficient, as related to the d_{ij} piezoelectric strain moduli by the elastic stiffness coefficients c_{ij}, the ferroelastic literature generally follows the convention that spontaneous strain is represented by the symbol e_s; this convention is followed here.

from about 0.003 for $NaH_3(SeO_3)_2$ to 0.257 for $KClO_3$. Additional values are to be found in the literature. The thermal dependence of e_s [*i.e.* $(1/e_s)(de_s/dT)\,K^{-1}$] has been reported less frequently; values for six representative crystals range from -5 to $-190 \times 10^{-4}\,K^{-1}$ (Abrahams, 1985). As the higher-symmetry phase is approached, the magnitude of e_s necessarily decreases, becoming zero at the phase transition; de_s/dT is hence generally negative.

3. *Group–subgroup relationship*

The transition from a ferroelastic to a higher-temperature phase is generally from lower to higher symmetry. The higher-symmetry phase is usually paraelastic (without spontaneous strain). If there is no integral change in any lattice dimension at the transition, the ferroelastic phase forms a subgroup of the paraelastic point group. A systematic tabulation of the corresponding group–subgroup relationships has been given by Salje (1990).

4. *Elastic hysteresis*

All as-grown ferroelastic crystals, in the absense of an applied stress, contain domains related to the two or more permissible lattice orientations derived from the higher-symmetry paraelastic lattice. These domains are initially present with an equal probability, and the walls between them are often readily observable in polarized light. The resulting net spontaneous strain in the as-grown crystal is hence close to zero as a result of mutual stress cancellation. The application of a compressive or shear stress, with magnitude greater than the coercive value, along a direction that converts one lattice orientation into another simultaneously reorients one set of domains, thereby increasing the net spontaneous strain to its maximum. The resulting single domain exhibits the full magnitude e_s. The spontaneous strain may be reoriented by the reapplication of stress along the appropriate direction, and the resulting stress–strain variation follows a normal hysteresis loop as illustrated by Fig. 7. The domain-wall motion observable in an as-grown ferroelastic crystal using an optical microscope as the applied stress is slowly increased is strikingly comparable to that seen in a polydomain ferroelectric crystal as an applied electric field is gradually increased, see § VI.3.

5. *Detwinning ferroelastic crystals*

As noted in § VIII.4, single-domain material may be produced from an as-grown ferroelastic crystal by the application of stress. If the required coercive stress exceeds the cohesive strength at a given temperature, the crystal will rupture before it is detwinned. It may hence be necessary to heat the crystal to higher temperatures before attempting the detwinnng process and subsequent formation of a single domain. Many ferroelastic crystals of interest are small and require the use of microtechniques for successful detwinning. A simple cell for achieving a single-domain ferroelastic crystal with transition temperatures ranging from 300 to 1300 K in a controlled atmosphere has been described by Abrahams, Bernstein, Chaminade & Ravez (1983); this cell has been used for detwinning crystals of several materials, including atmosphere-sensitive $Na_5W_3O_9F_5$ and $Rb_2KMoO_3F_3$, which decompose at higher temperatures in the presense of water vapor. A structure determination based on a detwinned ferroelastic crystal is generally more reliable than one based on modeling the twinning, particularly when the displacement Δ between ferroelastically related atoms (see § IX.1) is comparable to or greater than the r.m.s. displacement amplitudes associated with each atom. Results obtained by other physical measurements on detwinned samples of ferroelastic materials are also more intrinsically characteristic than those on twinned samples.

6. *Property coupling*

The development of ferroelasticity in a crystal below a phase transition from higher symmetry is often accompanied by the appearance of other tensor properties as a result of the coupling between e_s and the thermodynamic order parameter, and the resulting elastic softening of the crystal, see *e.g.* Tolédano & Tolédano (1987) and Salje (1990). In the event of coupling, reorientation of e_s causes reorientation of the other property and *vice versa*. For example, $Tb_2(MoO_4)_3$ is a coupled ferroelastic–ferroelectric crystal in which reorientation of e_{12} by applying a compressive stress of about $1.5\,MN\,m^{-2}$ along [010] at room temperature in the short-circuit case, or about $50\,MN\,m^{-2}$ in the open-circuit case, simultaneously exchanges the a and b axes as the sense of P_s is reversed along [001];

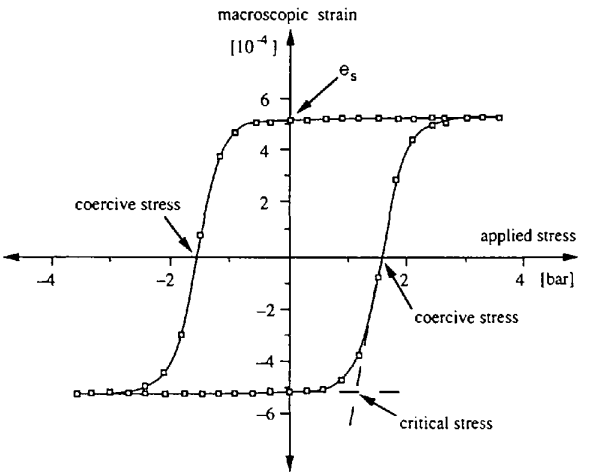

Fig. 7. Stress–strain hysteresis in $Pb_3(PO_4)_2$ (after Salje, 1990).

similarly, a d.c. coercive field of 400 kV m^{-1} along [001] simultaneously reorients e_{12} (Keve, Abrahams, Nassau & Glass, 1970), see also § VII.4. The spontaneous strain in $Tb_2(MoO_4)_3$ has been shown to be linearly proportional to the spontaneous polarization. Other coupled properties include piezoelectricity, optic effects, ferro- and ferrimagnetism.

Coupling between ferroelasticity and other physical properties is not required. For example, no coupling need be present in a crystal with a phase transition from a piezoelectric paraelastic phase to a lower-temperature piezoelectric ferroelastic phase, as in the case of $K_2Cd_2(SO_4)_3$, see § IX.2.

IX. Structure and ferroelasticity

1. *Atomic displacement and e_s*

Reorientation of the spontaneous strain is a consequence of an atomic distribution reorientation. As noted in § VIII.2, ferroelastic crystals always have lattice parameters that are only a small distortion from a higher symmetry, see also (10). In addition, the atomic distribution must be such that pairs of like atoms located at (x_1, y_1, z_1) and (x_2, y_2, z_2) are pseudosymmetrically related by

$$(x_1, y_1, z_1) = f(x_2, y_2, z_2) + \Delta, \qquad (11)$$

where Δ is an atomic displacement on the order of 1 Å and $f(x_2, y_2, z_2)$ is a transformation that results in a reorientation of the lattice vectors. For example, if a phase transition from tetragonal symmetry results on cooling to give an orthorhombic crystal in which the distortion from higher symmetry is small, then a common transformation $f(x_2, y_2, z_2)$ such as that given by

$$(x_1, y_1, z_1) = \left(\tfrac{1}{2} - y_2, \tfrac{1}{2} + x_2, z_2\right) + \Delta \qquad (12)$$

may be interpreted as indicating that the a and b axes are interchangeable, with a reversal in the sense of the transformed a axis, assuming normal displacements (*i.e.* $\Delta < \sim 1$ Å) by each atom. The transformation in (12) is equivalent to $0\bar{1}0/100/001$.

Ferroelasticity is a widespread but still relatively underinvestigated property. Two ferroelastics have already been considered in this article, $BaTiO_3$ in § VII.2 and $Tb_2(MoO_4)_3$ in § VII.4, each with a normal range of atomic displacements. The largest values reported for the magnitude of Δ are comparable in length to the lattice parameters. In 9-hydroxy-1-phenalenone, for example, ferroelastic transformation of the a, c axes is accompanied by both molecular rotations with Δ_{max} about 1.43 Å and a translation of inversion centers by about 7.68 Å (Svensson & Abrahams, 1984). Three families of ferroelastics are now considered further to illustrate the structure–property relationship. Each is derived from a cubic prototype.

2. *The langbeinite family*

This family has formula $A^{+}{}_2M^{2+}{}_2(SO_4{}^{3-})_3$ with A = NH_4, K, Rb, Cs, Tl and M = Mg, Ca, Mn, Fe, Co, Ni, Zn, Cd. The high-temperature phase of all members reported has space group $P2_13$. Four structural transitions are possible, to space groups $R3$, $P2_12_12_1$, $P2_1$ and $P1$. The first three involve improper ferroelectric transitions. The change of phase from $P2_13$ to $P2_12_12_1$ involves a ferroelastic transition, as found in all langbeinites with A = K and each of the above M atoms. The member with M = Cd is considered here as typical: $K_2Cd_2(SO_4)_3$ has a = 10.208 2 (2), b = 10.283 7 (3) and c = 10.166 1 (1) Å at 298 K with a transition to cubic $P2_13$ at 432 K with a = 10.267 5 (10) Å (Abrahams, Lissalde & Bernstein, 1978; Lissalde, Abrahams, Bernstein & Nassau, 1979). The spontaneous strain at 298 K derived from the lattice-parameter magnitudes is small, with $e_{12} = 3.68 \times 10^{-3}$, $e_{13} = 2.07 \times 10^{-3}$ and $e_{23} = 5.75 \times 10^{-5}$. Ferroelastic reorientation at 298 K has not been achieved but a compressive stress of 5 MN m^{-2} applied along [010] at 435 K followed by cooling while still under this stress resulted in unit-cell reorientation as given by the transformation 010/001/100.

Independent pairs of like atoms in $K_2Cd_2(SO_4)_3$ below the phase-transition temperature with coordinates (x_1, y_1, z_1) and (x_2, y_2, z_2) are pseudosymmetrically related:

$$(x_1, y_1, z_1) = (y_2, z_2, x_2) + \Delta \qquad (13)$$

with $0.262 \leq \Delta \leq 1.190$ Å at 298 K, where Δ is the sum of the Δx, Δy, Δz displacements. It may be seen from (13) that the atomic basis for ferroelectric reorientation, in which the original a axis is replaced by b, the original b axis by c and the original c axis by a, confirms the experimental transformation given above. Percival (1990) has found that the phase transition order parameter is not linearly coupled to e_s in $K_2Cd_2(SO_4)_3$, so that this langbeinite may be classified as an improper ferroelastic. Proper ferroelastics are defined as those in which e_s is linearly proportional to the order parameter. The space group $P2_13$ above the ferroelastic–paraelastic phase transition, however, is suggestive of a group–subgroup relationship and hence formation of a proper ferroelastic.

The structure of $K_2Cd_2(SO_4)_3$ at four temperatures below and one above the phase transition T_c (Abrahams, Lissalde & Bernstein, 1978) and that of a Co-doped $K_2Cd_2(SO_4)_3$ crystal at three temperatures above T_c (Percival, Schmahl & Salje, 1989) led to the conclusion that the nonlinear coupling is associated with local scale distortions in the MO_6 octahedra. Well above T_c, Percival (1990) proposes a symmetrical octahedron is formed but

with a displaced central M^{2+} cation; as the temperature falls, instabilities at the large A sites increase and the arrangement of O atoms around these sites changes as the average A–O distance decreases, resulting in octahedral distortions. The variation in M–O bond length decreases closer to T_c as the coordination number at the A sites changes, thereby providing a trigger for the phase transition. The information and accompanying insight available by determining the full structural thermal dependence of ferroelastic materials over a temperature range that includes the phase transition, as in the case of $K_2Cd_2(SO_4)_3$, provides a useful investigative model for other ferroelectrics.

3. $SmAlO_3$ *and* $LaFeO_3$

Many materials derived from the cubic ABO_3 perovskite structure with point group $m\bar{3}m$ exhibit small distortions from this higher symmetry. The noncentrosymmetric point groups $4mm$, $mm2$ and $3m$ and the corresponding centrosymmetric point groups are found among the possible lower-symmetry forms. Ferroelectricity is common among the derivative materials with point groups lacking an inversion center, and these will not be discussed further in this section (but see § VII.2 for $BaTiO_3$). $SmAlO_3$ and $LaFeO_3$ are typical of those materials having an orthorhombic distortion and an inversion center in space group $Pbnm$. The lattice parameters of $SmAlO_3$ at 298 K are a = 5.291 08 (2), b = 5.290 48 (2), c = 7.474 20 (5) Å, with $e_{12} = 56.3 \times 10^{-6}$. The latter material is similar, with $e_{12} = 238 \times 10^{-6}$. Within the unit cell of an untwinned crystal of either, each atom at (x_1, y_1, z_1) is related to a like atom at (x_2, y_2, z_2) by the relationship

$$(x_1, y_1, z_1) = (-y_2, x_2, z_2) + \Delta \qquad (14)$$

with $0.184 \leq \Delta \leq 0.642$ Å for $SmAlO_3$ and $0.228 \leq \Delta \leq 0.790$ Å for $LaFeO_3$ (Abrahams, Bernstein & Remeika, 1974).

Equation (14) shows that ferroelastic reorientation results in an interchange of the a and b axes corresponding to the transformation $0\bar{1}0/100/001$. Experimentally, the application of a compressive stress of $\sim 50\,MN\,m^{-2}$ normal to (100) causes the expected axial reorientation in $SmAlO_3$. The stress required to reorient the two axes in $LaFeO_3$ is $\sim 300\,MN\,m^{-2}$; the coercive stress in these and many materials is sensitive both to defect distribution and atomic displacement.

It may be noted that the macroscopic spin configurations associated with the magnetic ions located along the a and b axes in these materials are necessarily also rotated on ferroelastic reorientation. The magnetic properties of these materials are hence ferroelastically coupled; such couplings remain underinvestigated and offer a promising new field for study by either neutron or synchrotron X-ray diffraction techniques.

4. K_2TeBr_6 *and the antifluorite family*

Numerous hexahalometallates of formula A_2BX_6, where A is an alkali, B a tetravalent metal and X a halogen atom, crystallize with the cubic K_2PtCl_6 antifluorite structure in space group $Fm\bar{3}m$ and many undergo one or more phase transitions at lower temperatures. Many of these phases are expected to be ferroelastic, in view of their small distortions from cubic, as was found to be the case for K_2TeBr_6. At 435 K, the latter has a cubic lattice parameter a = 10.745 6 (14) Å, with a reduction in symmetry to tetragonal below T_{c1} = 434 K, with a = 7.575 5 (10), c = 10.770 2 (22) Å at 410 K, and to monoclinic below T_{c2} = 400 K with a = 7.490 8 (10), b = 7.549 2 (7), c = 10.698 4 (11) Å and β = 90.307 (6)° at 295 K (Abrahams, Ihringer, Marsh & Nassau, 1984), for a corresponding $e_{12} = 3.88 \times 10^{-3}$. The higher-temperature phase-transition temperature is denoted by T_{c1}, the lower by T_{c2}. The lattice-parameter dependence on temperature over the range 20 to 463 K is shown, together with the corresponding heat-capacity variation between 266 and 450 K in Fig. 8.

The coupling between elastic strain (e) and order parameter (Q) in K_2TeBr_6 has been investigated by group-theoretical normal-mode analysis. Two effective modes have been identified in the tetragonal phase, one producing a displacement of the K^+ ions, the other a rotation of the $TeBr_6^{2+}$ octahedra (Ihringer & Abrahams, 1984). Lattice distortion results from the coupling between Q and e, with $e_{13} \propto Q$ and, independently, $e_{22}-e_{11} \propto Q^2$; the heat-capacity change in Fig. 8 is caused primarily by the quadratic coupling. One mode condenses at T_{c2} with $e_{13} \propto (400\,K - T)^{1/2}$ leaving $e_{22}-e_{11} = 0$ for $359 < T < 400$ K; below 359 K, $e_{22}-e_{11} \propto (359\,K - T)$. By contrast, the transition at T_{c1} has a single soft mode that leaves the K-atom special position unchanged. The small distortion from cubic to the monoclinic lattice parameters above suggests the possibility of ferroelasticity. Examination of the corresponding atomic coordinates shows that each atom at (x_1, y_1, z_1) is indeed ferroelastically related to another atom of the same kind at (x_2, y_2, z_2) by

$$(x_1, y_1, z_1) = (y_2, -x_2, z_2) + \Delta \qquad (15)$$

with $0 \leq \Delta \leq 0.613$ Å. This displacement range is rather small and may be expected to correspond to a small coercive stress along [010] sufficing to interchange the **a** and **b** axial vectors in accordance with the transformation $010/\bar{1}00/001$, as inferred from (15). Although it has not been measured accurately, E_{12} has been experimentally estimated as on the order of $10^6\,N\,m^{-2}$.

5. *Other ferroelastics*

A list of nearly 200 ferroelastics reported in the literature prior to about 1989, with their transition temperatures where available, has been compiled by Salje (1990).

6. *Criteria for identifying new ferroelastics*

Numerous materials investigated in the past for unrelated reasons may be expected to exhibit ferroelasticity but have not yet been identified as such. There are two readily applicable structural criteria for the identification of new ferroelectrics from data in the literature; determination of the requisite experimental proof is likewise readily made. All ferroelastics are necessarily closely related to, but undergo a small distortion from, higher symmetry. The first criterion is hence that the lattice distortion, as given by the e_{ij} moduli appropriate for the symmetry of the given crystal, be no greater than $\sim 10^{-3}$. The second criterion is that the atomic coordinates satisfy the relationship given in (11) with no value of Δ that exceeds ~ 2.5 Å. Smaller values of Δ offer a greater chance that the crystal is indeed ferroelastic. It may be noted that the space group of the candidate material generally satisfies a subgroup–group relationship in the event that there is no integral change in lattice parameter at the higher-temperature phase transition.

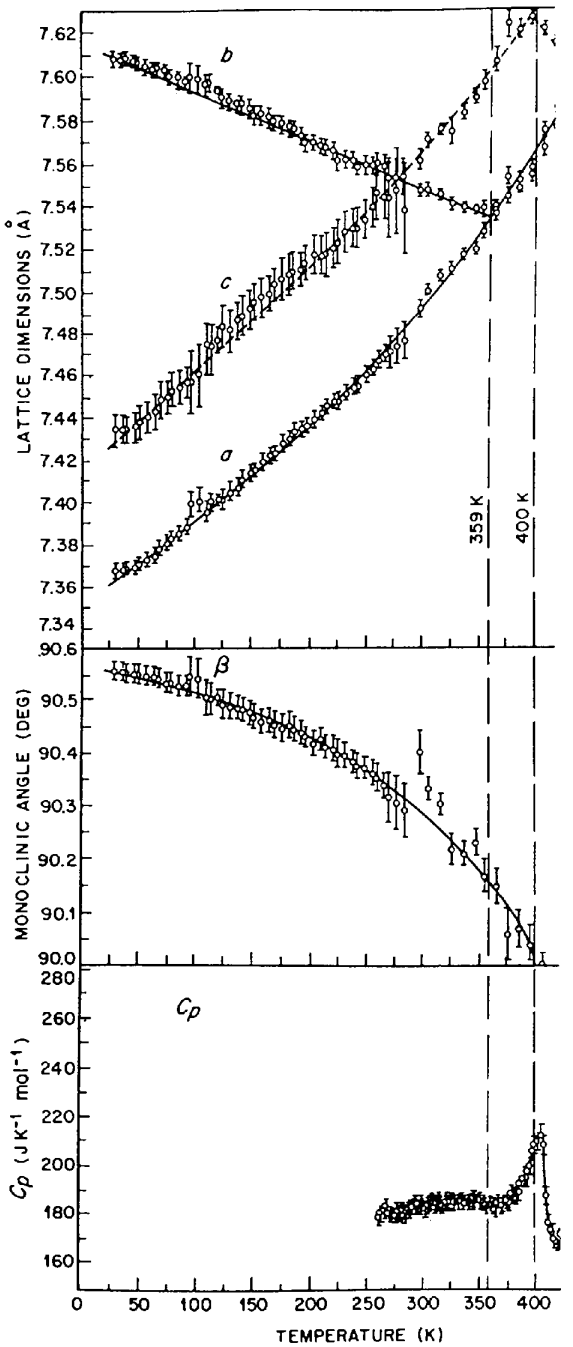

Fig. 8. Lattice-parameter and heat-capacity temperature dependence of K_2TeBr_6 between 20 and 400 K (after Abrahams, Ihringer, Marsh & Nassau, 1984).

Crystals that satisfy these two criteria must also be shown to demonstrate ferroelastic behavior before they can be accepted as new ferroelastics. Ferroelastic crystals generally exhibit a characteristic domain pattern on examination under polarized light. This pattern is usually sensitive to the application of external stress on the order of 1 MN m^{-2} (see §§ III.6 and VIII.2 for applied finger pressure). Minimum proof of ferroelasticity requires a reproducible change in the domain pattern under such an application of stress, with further change observable on releasing the stress. Production of a single domain from a multidomain crystal, an unambiguous X-ray diffraction demonstration of ferroelastic interchange by the crystal axes or the observation of ferroelastic hysteresis provide successively higher levels of confidence that the new material is ferroelastic.

X. Optical activity and crystal chirality

1. *Optical rotatory power*

Plane-polarized light transmitted through noncentrosymmetric crystals is rotated through an angle proportional to the crystal thickness traversed, except for crystals with classes $4mm$, $\bar{4}3m$, $3m$, $6mm$, $\bar{6}$ or $\bar{6}2m$ in which all coefficients of the second-rank axial gyration tensor have zero value, see *e.g.* Nye (1957). The gyration tensor, with its maximum of six independent coefficients in crystal class 1, relates the amount of optical activity to crystal direction. The rotation is caused by the incident plane-polarized light splitting into two circularly polarized waves of opposite handedness on entering the crystal. The handedness or chirality of an enantiomorphic crystal causes a velocity difference between the two circularly polarized components leading to a resulting rotation of the polarization plane observed leaving the crystal. The sense of the rotation is given by the sense of the faster of the two circularly polarized components. The rotatory power $\rho = \varphi/d$, where φ is the rotation of the plane of polarization and d is the distance traversed in the crystal, is related to the refractive indices

n for right- (r) and left- (l) handed waves by $\rho = (\pi/\lambda_0)(n_l - n_r)$, where λ_0 is the wavelength of the light in a vacuum. The value of $n_l - n_r$ is on the order of 10^{-4} or less for most optically active crystals. Optical activity is generally most readily studied in the absence of birefringence, which often masks the former much smaller effect, close to an optic axis.

2. *Measurement of optical activity*

Optical rotatory power is readily measured in principle by use of a pair of rotatable polarizers and a lens system capable of producing accurately collimated parallel light. Although white light may be used, the inability to reach complete extinction at all positions of the crossed polarizers due to rotatory dispersion and the color change due to selective frequency transmission makes the use of monochromatic light preferable. A typical measurement incorporates a focused monochromatic laser (*e.g.* He–Ne) beam, with polarizers and detector in the optical path. Since ρ is dependent upon λ_0, the measurement is generally made over a range of wavelengths as well as crystal thicknesses. Crystal plate samples should always be examined carefully for the possible presence of opposite chirality domains, by spatially filtering and expanding the laser beam to cover the entire crystal. Values reported for ρ range from 1 to 10^3 ° mm^{-1}. An optically laevorotatory (−) crystal rotates the plane of polarization counterclockwise as detected by an observer facing the light source, a dextrorotatory (+) crystal rotates the plane clockwise. Contrastingly, the sense of structural screws in the crystal are conventionally taken in the direction leaving the observer, see also § XI.1. Other definitions relevant to optical activity are listed by Glazer & Stadnicka (1986).

3. *Absolute-chirality determination*

Application of the techniques used in §§ II.5, IV.5 and VI.4 for the determination of the absolute atomic arrangement to a crystal of known chirality, see § X.2, gives the absolute chirality. It is always advisable to remeasure the chirality of the crystal to be used in the diffraction experiment before undertaking an absolute-structure determination.

XI. Structure and crystal chirality

1. *Structural origin of optical activity*

Two basic theories have slowly developed, over many years, to account for the origin of optical activity on the basis of crystal structure; one is based on electromagnetic theory and the other on atomic polarizabilities. Glazer & Stadnicka (1986) have presented a brief historical review of this development together with an extension of the latter theory as advanced by Ramachandran (1951). They have shown, for a series of enantiomorphic crystals, that the optical-rotation sense of each may be determined from an examination of its absolute structure by assuming four conditions: (*a*) that the primary contribution to the optical activity is caused by the most highly electronically polarizable of the atoms present; (*b*) that the shortest vectors between polarizable atoms correspond to the direction of highest polarizability; (*c*) that the optical activity is greatest for helices with the shortest interatomic distances and lowest pitches; and (*d*) that the sign of ρ is determined by the directions of the anisotropic polarizabilities in the plane perpendicular to the helix axis, with the incident polarized light rotating in the same direction as the larger polarizability component tangential to the helix. It should be noted with care that convention describes the chirality of a structural screw as it moves away from the observer, whereas the chirality of optical rotation is described in terms of the wave front moving toward the observer; the structural screw is hence described with a sense opposite to that of the optical rotation.

The relationship between atomic arrangement and optical activity is analogous to that between light transmission and optical waveguides. In the latter, light is confined to propagation through a higher-refractive-index medium by means of internal reflection at the interface with the surrounding lower-index medium. In the former, the circularly polarized component of the entering plane-polarized light source is confined to propagation along a helix bounded by regions of higher polarizability; the wave front propagates with higher velocity for the component with spatial handedness matching that of the helix. Although the following model has not been fully developed quantitatively, it is likely that the larger the helix area defined by conditions (*c*) and (*d*) above, the higher will be the fraction of matching circularly polarized component passing through the crystal with resulting higher value of ρ, since each helix acts as a conducting light pipe to maximize the interaction between wave front and structural screw, see also Devarajan & Glazer (1986).

Glazer & Stadnicka (1986) successfully applied their four conditions to nine optically active materials for which the absolute chirality had been determined without ambiguity, including α-quartz, α-$AlPO_4$, α-HgS and $Ca_2Sr[C_2H_5COO]_6$, in addition to the materials in the following three sections. The total number of optically active materials for which reliable structural chirality results are available, although small, is growing and Glazer & Stadnicka's (1986) analysis has also been applied by these authors to α-$NiSO_4{\cdot}6H_2O$, $Bi_{12}TiO_{20}$, $ZnSeO_4{\cdot}6H_2O$, α-TeO_2, $Ba(NO_2)_2{\cdot}H_2O$, $SrS_2O_6{\cdot}4H_2O$, $KTiPO_4$, $NH_4H_2PO_4$ and $KLiSO_4$ among others. It may be observed that the experimental determination of absolute chirality has, in the past, been beset by numerous

errors. By their nature, absolute-sign determinations are always either right or wrong.

2. *Absolute chirality of* $Bi_{12}SiO_{20}$ *and* $Bi_{12}GeO_{20}$

The nonlinear optical properties of these two cubic materials with space group $I23$ and $a \simeq 10.1$ Å, often referred to as BSO and BGO, respectively, has led to their commercial growth in the form of large single-crystal boules. The absolute chirality of BSO and BGO was determined by measuring their crystal structures on small spheres ground from large laevorotatory boules (Abrahams, Svensson & Tanguay, 1979). BSO and BGO have comparable values of ρ that range from 60 to $20° \text{ mm}^{-1}$ for λ between 4500 and 6500 Å. Glazer & Stadnicka (1986) estimate that the polarizability of the O^{2-} ion greatly exceeds that of Bi^{3+} or Si^{4+} (or Ge^{4+} which they do not discuss in detail), hence the contribution from the cations may be neglected on the basis of their initial condition. The helices formed by two of the three crystallographically independent oxygen atoms, O2 and O3, about the 3_1 axes in the BSO structure are readily seen in Fig. 9(*a*). Both helices, however, not only contain long O2–O2 and O3–O3 distances, at 5.29 and 6.74 Å, which most likely contribute little to the optical activity but that contribution is exactly cancelled by equivalent helices formed about the 3_2 axes. Bi also forms two helices of opposite chirality that essentially cancel.

The only remaining atom that can contribute to the optical activity is O1, which forms two helices consisting of short O1–O1 distances; the helix close to the 3_1 axis has O–O = 3.057 Å and that about the 3_2 axis has O–O = 3.168 Å. Applying their second condition, Glazer & Stadnicka regard the former (*ABC* in Fig. 9*b*) as making the dominant contribution to the optical activity. Fig. 9(*b*) also shows (dotted) the inferred O1 polarizability ellipsoids, which are oriented close to tangential with respect to the right-handed screw *ABC* helix. This relatively complicated structure is hence fully consistent with the laevorotatory crystal on which the structure was measured, since a structurally right-handed screw helix matches the chirality of a left-handed optical rotation.

The absolute atomic arrangement in $Bi_{12}GeO_{20}$ is very similar to that in BSO, with slightly larger O1–O1 distances of 3.07 Å in the right-handed screw helix close to the 3_1 axes and Ge^{4+} polarizability comparable to that of Si^{4+}. This structure is hence also expected to be laevorotatory, as observed experimentally.

3. *Chirality of* $NaClO_3$ *and* $NaBrO_3$

The structures of these two cubic crystals, with space group $P2_13$ and $a = 6.575\,84$ and $6.707\,17$ Å, respectively, were first reported in the 1920's and subsequently have been extensively reinvestigated. An 1856 observation by Marbach suggesting that the same structural configuration leads to the opposite optical rotation sense was supported by Beurskens-Kerssen, Kroon, Endeman, van Laar & Bijvoet (1963) and later confirmed by Abrahams, Glass & Nassau (1977). With total polarizabilities of 5.3 $Å^3$ for $NaClO_3$ and 6.5 $Å^3$ for $NaBrO_3$, and only about 0.2 $Å^3$ for Na^+, Glazer & Stadnicka's (1986) first condition suggests that the Na-atom contribution may be neglected. The 1977 atomic coordinates for the laevorotatory form of both compounds reveals two types of helix in $NaClO_3$. The highest polarizability direction as required by their second condition is given by the shortest O–O contacts pointing toward the O_3 helix center, marked in Fig. 10(*a*) by the long axes of the

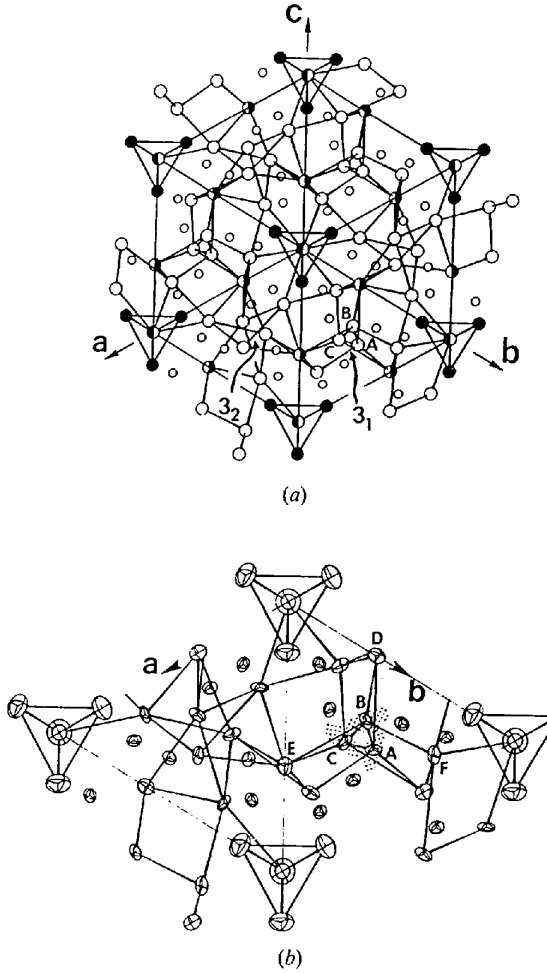

Fig. 9. (*a*) View of the structure of $Bi_{12}SiO_{20}$ along the body diagonal, with smaller circles representing Bi, larger filled circles O3, half-filled circles O2 and larger open circles O1 and all O–O connections less than 3.1 Å shown. (*b*) Enlarged upper part of view, with polarizability ellipsoids near 3_1 axis shown dotted. O–O distances are BF = 2.738, BD = 2.777, BE = 3.057, BC = BA = CA = 3.059 Å (after Glazer & Stadnicka, 1986).

polarizability ellipsoids, which are shown dotted. Although the four-atom *DEFG* helix might be expected to produce a larger optical rotation than the three-atom *ABC* helix with identical polarizabilities, the third condition suggests that the smaller polarizability of the Cl atom reduces the former's relative contribution. Taking the sense of each helix from the tangential polarizability ellipsoids, as shown in the figure by the arrows, the fourth condition gives the respective optical-rotation directions of both. On summing the two, the contribution from the right-handed screw helices predominates resulting in a slightly laevorotatory optical rotation direction, in agreement with experiment.

Fig. 10(*b*) shows that the structure of a crystal of $NaBrO_3$ with opposit chirality leads to a similar situation, with a helix *EAFD* consisting of –Br–O–Br–O– atoms along the 2_1 axis and a helix *ACB* of O atoms. The larger polarizability of Br results in the *EAFD* helix having the larger optical rotation, hence the crystal is again predicted to be laevorotatory, in accordance with experiment.

4. *Chirality of* α-$LiIO_3$

The piezoelectric and pyroelectric properties of α-$LiIO_3$ are closely related to the atomic arrangement in the solid state, see §§ III.4 and V.3. Both enantiomorphic forms grow from solution, as expected for space group $P6_3$. Determination of the absolute configuration shows that the iodine apices of the iodate ions point in the direction of the steeper (+c) ends of each crystal, with an iodate-ion rotation of about 30° about the trigonal axis between the two absolute chiral forms (Svensson, Albertsson, Liminga, Kvick & Abrahams, 1983). The

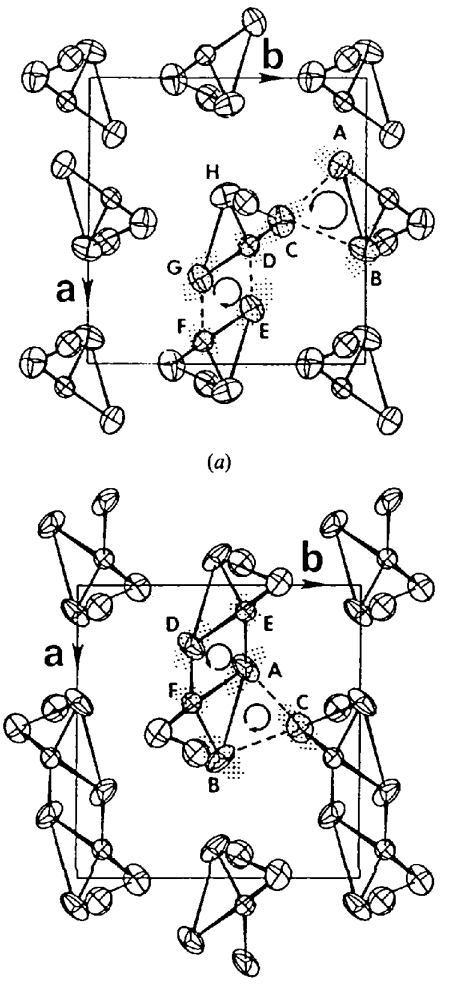

Fig. 10. (*a*) Projection of the structure of laevorotatory $NaClO_3$ on (001), showing O atoms at *A*, *B*, *C*, *E*, *G* and H and Cl atoms at *D* and *F*, with Na atoms omitted. The *BAC* helix forms a right-handed screw, the *DEFG* helix a left-handed screw. (*b*) Same projection of laevorotatory $NaBrO_3$, with O atoms at *A*, *B*, *C* and *D* and Br atoms at *E* and *F* (after Glazer & Stadnicka, 1986).

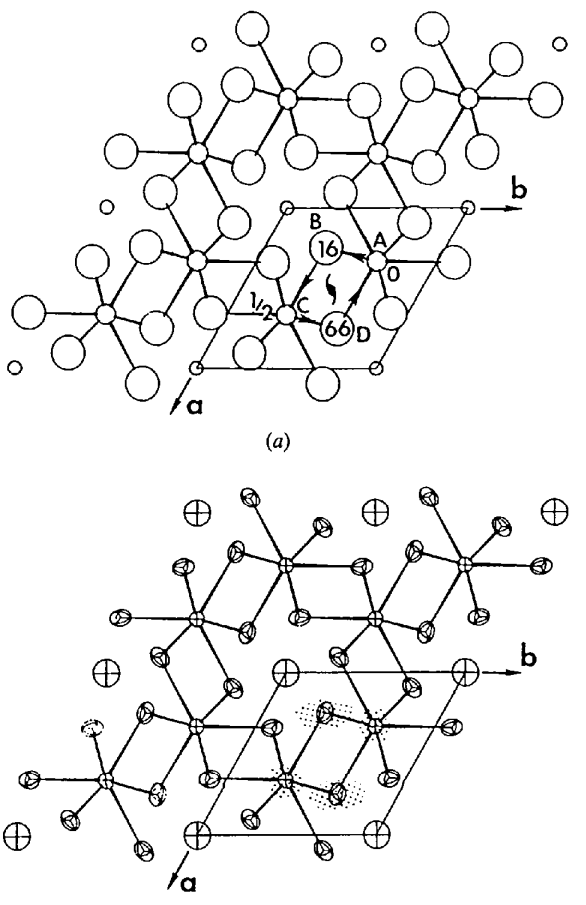

Fig. 11. (*a*) Projection of the structure of laevorotatory α-$LiIO_3$ along the polar *c* axis. The larger circles (*B* and *D*) represent oxygen, intermediate circles (*A* and *C*) iodine and small circles lithium. The heights of *B* and *D* are given in units of *c*/100. (*b*) The polarizability ellipsoids tangential to the *ABCD* helix are indicative of a laevorotatory structure (after Glazer & Stadnicka, 1986).

latter did not make optical measurements on α-$LiIO_3$ but relied on the relation between chirality and optical rotation proposed by Li (1981), based on his optical rotation and X-ray dispersion results, to determine the absolute chirality. Glazer & Stadnicka (1986) found the resulting chirality to be inconsistent with the conditions in § XI.1. Stadnicka, Glazer & Moxon (1985) subsequently demonstrated Li's results to be in error. The atomic coordinates determined by Svensson *et al.* (1983) hence correspond to the dextrorotatory form. The signs of the z coordinates are reversed in Fig. 11(*a*), and the atomic arrangement shown there corresponds to the laevorotatory form.

Noting that most of the optical polarizability in α-$LiIO_3$ results from the IO_3^- ion, Glazer & Stadnicka (1986) neglect further consideration of Li^+ in Fig. 11(*a*). The polarizability ellipsoids for the O atoms are assumed to lie along the shorter I–O distances (*AB*), shown dotted in Fig. 11(*b*) and approximately tangential to the *ABCD* helix, which forms a right-handed screw. The optical-rotation sense, which for normal dispersion is opposite that of the structural handedness for the case with largest component polarizabilities tangential to the helix, is hence laevorotatory in accordance with the absolute chirality.

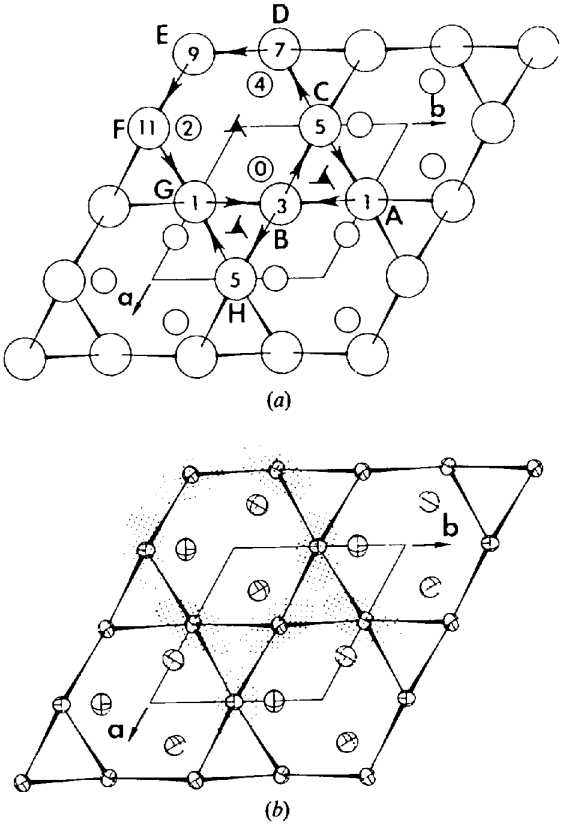

Fig. 12. (*a*) Projection of the structure of laevorotatory α-HgS along the trigonal c axis. Small circles represent Hg, large ones S atoms, with heights marked in units of $c/6$. The *BHG* helix forms a left-handed screw, the *BCDEFG* helix a right-handed screw. (*b*) Both the polarizability ellipsoids tangential to the *BCDEFG* helix and those radial to the *BHG* helix indicate a laevorotatory structure (after Glazer & Stadnicka, 1986).

5. *Chirality of* α-HgS

This intensely red material, also known as cinnabar or vermillion, crystallizes in space group $P3_221$ with $a = 4.145$ and $c = 9.496$ Å. Its structure rather clearly illustrates the importance of the major anisotropic polarizability component direction. If the component tangential to the helix axis is largest, then the incident light is rotated in the same sense as the helix; if the radial component is largest, then the incident light is rotated in the opposite sense to that of the helix. The atomic arrangement determined by Auvray (1976) is shown in Fig. 12(*a*), as projected along the trigonal axis. With isotropic polarizabilities of 1.24 $Å^3$ for Hg^{2+} and 10.3 $Å^3$ for S^{2-}, Glazer & Stadnicka (1986) infer that the S-atom contribution dominates the total polarizability, hence Fig. 12(*a*) shows only the short S–S distances, which lead to the directions of highest polarization marked in Fig. 12(*b*). The structure contains two independent helices, one around the screw axis at $(0, 0, z)$ and the other around $(2/3, 1/3, z)$. The former is a right-handed screw with tangential polarizability ellipsoids, the latter is a left-handed screw with radial polarizability ellipsoids. Incident light travelling along the former is expected to undergo the same sense of rotation, *i.e.* left handed towards the observer. Incident light transmitted along the latter helix is expected to undergo the opposite sense of rotation, *i.e.* right-handed toward or left-handed away from the observer. Both types of helix (it may be noted that there are twice as many of the latter as the former within the α-HgS unit cell) hence act similarly on incident plane polarized light to give the large observed laevorotatory optical rotation.

6. *New absolute determinations of chiral structures*

Numerous enantiomorphic crystal-structure determinations are reported in the crystallographic literature; a promising new research area clearly lies in accompanying such investigations with a determination of the absolute chirality of the sample material, followed by the application of Glazer & Stadnicka's (1986) optical rotation analysis.

It is a pleasure to thank Dr Y. Le Page for valuable discussions concerning α-quartz, Dr E. N. Maslen for helpful comments on $BaTiO_3$, Dr A. M. Glazer for pointing out many recent structural determinations of absolute chirality, a referee for suggesting the inclusion of § XI.5 and Professor A. Authier for his perceptive and clarifying observations on the manuscript.

References

ABRAHAMS, S. C. (1971). *Mater. Res. Bull.* **6**, 881–890.

ABRAHAMS, S. C. (1975). *Anomalous Scattering*, edited by S. RAMASESHAN & S. C. ABRAHAMS, pp. 199–221. Copenhagen: Munksgaard.

ABRAHAMS, S. C. (1978). *Mater. Res. Bull.* **13**, 1253–1258.

ABRAHAMS, S. C. (1985). *Aust. J. Phys.* **38**, 289–298.

ABRAHAMS, S. C. (1988). *Acta Cryst.* B**44**, 585–595.

ABRAHAMS, S. C. (1989). *Acta Cryst.* B**45**, 228–232.

ABRAHAMS, S. C., ALBERTSSON, J., SVENSSON, C. & RAVEZ, J. (1990). *Acta Cryst.* B**46**, 497–502.

ABRAHAMS, S. C., BARNS, R. L., BERNSTEIN, J. L. & TURNER, E. H. (1974). *Solid State Commun.* **15**, 737–739.

ABRAHAMS, S. C. & BERNSTEIN, J. L. (1969). *Acta Cryst.* B**25**, 1233–1236.

ABRAHAMS, S. C. & BERNSTEIN, J. L. (1973). *J. Chem. Phys.* **59**, 1625–1629.

ABRAHAMS, S. C. & BERNSTEIN, J. L. (1979). *J. Appl. Cryst.* **12**, 425–426.

ABRAHAMS, S. C., BERNSTEIN, J. L., CHAMINADE, J. P. & RAVEZ, J. (1983). *J. Appl. Cryst.* **16**, 96–98.

ABRAHAMS, S. C., BERNSTEIN, J. L. & REMEIKA, J. P. (1974). *Mater. Res. Bull.* **9**, 1613–1616.

ABRAHAMS, S. C., BUEHLER, E., HAMILTON, W. C. & LAPLACA, S. J. (1973). *J. Phys. Chem. Solids*, **34**, 521–532.

ABRAHAMS, S. C., GLASS, A. M. & NASSAU, K. (1977). *Solid State Commun.* **24**, 515–516.

ABRAHAMS, S. C., IHRINGER, J., MARSH, P. & NASSAU, K. (1984). *J. Chem. Phys.* **81**, 2082–2087.

ABRAHAMS, S. C. & KEVE, E. T. (1971). *Ferroelectrics*, **2**, 129–154.

ABRAHAMS, S. C., KURTZ, S. K. & JAMIESON, P. B. (1968). *Phys. Rev.* **172**, 551–553.

ABRAHAMS, S. C., LIMINGA, R. & ALBERTSSON, J. (1990). *J. Appl. Cryst.* **23**, 211–212.

ABRAHAMS, S. C., LIMINGA, R., MARSH, P., SCHREY, F., ALBERTSSON, J., SVENSSON, C. & KVICK, Å. (1983). *J. Appl. Cryst.* **16**, 453–457.

ABRAHAMS, S. C., LISSALDE, F. & BERNSTEIN, J. L. (1978). *J. Chem. Phys.* **68**, 1926–1935.

ABRAHAMS, S. C. & MARSH, P. (1986). *Acta Cryst.* B**42**, 61–68.

ABRAHAMS, S. C. & NASSAU, K. (1986). *Encyclopedia of Materials Science and Engineering*, edited by M. B. BEVER, pp. 3524–3528. Oxford/New York: Pergamon Press.

ABRAHAMS, S. C., RAVEZ, J., CANOUET, S., GRANNEC, J. & LOIACONO, G. M. (1984). *J. Appl. Phys.* **55**, 3056–3060.

ABRAHAMS, S. C., RAVEZ, J., SIMON, A. & CHAMINADE, J. P. (1981). *J. Appl. Phys.* **52**, 4740–4743.

ABRAHAMS, S. C., REDDY, J. & BERNSTEIN, J. L. (1966). *J. Phys. Chem. Solids*, **27**, 997–1012.

ABRAHAMS, S. C., SVENSSON, C. & BERNSTEIN, J. L. (1980). *J. Chem. Phys.* **72**, 4278–4285.

ABRAHAMS, S. C., SVENSSON, C. & TANGUAY, A. R. (1979). *Solid State Commun.* **30**, 293–295.

AIZU, K. (1969). *J. Phys. Soc. Jpn*, **27**, 387–396.

ALBERTSSON, J., ABRAHAMS, S. C. & KVICK, Å. (1989). *Acta Cryst.* B**45**, 34–40.

ANDRIAMAMPIANINA, V., GRAVEREAU, P., RAVEZ, J. & ABRAHAMS, S. C. (1994). *Acta Cryst.* B**50**, 135–141.

ARQUIS-CANOUET, S., RAVEZ, J. & ABRAHAMS, S. C. (1986). *J. Appl. Cryst.* **19**, 374–376.

AUVRAY, P. (1976). *Bull. Soc. Fr. Minéral. Crystallogr.* **99**, 373–378.

BAILEY, P. (1952). PhD thesis, Univ. of Bristol, England.

BAILEY, R. T., CRUICKSHANK, F. R., PUGH, D. & SHERWOOD, J. N. (1991). *Acta Cryst.* A**47**, 145–155.

BARNS, R. L. (1968). Private communication.

BERGMAN, J. G. & CRANE, G. R. (1974). *J. Chem. Phys.* **6**, 2470–2474.

BEURSKENS-KERSSEN, G., KROON, J., ENDEMAN, H. J., VAN LAAR, J. & BIJVOET, J. M. (1963). *Crystallography and Crystal Perfection*, edited by G. N. RAMACHANDRAN, pp. 225–236. London: Academic Press.

BHALLA, A. S. (1984). *J. Appl. Phys.* **55**, 1229–1230.

BRAGG, W. H. & BRAGG, W. L. (1915). *X-rays and Crystal Structure*. London: Bell.

BURFOOT, J. C. & TAYLOR, G. W. (1979). *Polar Dielectrics and their Applications*. Berkeley, CA: Univ. of California Press.

BUTTNER, R. H. & MASLEN, E. N. (1992). *Acta Cryst.* B**48**, 764–769.

CADY, W. G. (1964). *Piezoelectricity*. New York: Dover.

CALAGE, Y., ABRAHAMS, S. C., RAVEZ, J. & DE PAPE, R. (1990). *J. Appl. Phys.* **67**, 430–433.

Crystallographic Databases (1987). Bonn/Cambridge/Chester: International Union of Crystallography.

DEVARAJAN, V. & GLAZER, A. M. (1986). *Acta Cryst.* A**42**, 560–569.

DONNAY, J. D. H. & LE PAGE, Y. (1978). *Acta Cryst.* A**34**, 584–594.

EVANS, H. T. (1961). *Acta Cryst.* **14**, 1019–1026.

GLASS, A. M. (1969). *J. Appl. Phys.* **40**, 4699–4713.

GLAZER, A. M. & STADNICKA, K. (1986). *J. Appl. Cryst.* **19**, 108–122.

GLAZER, A. M. & STADNICKA, K. (1989). *Acta Cryst.* A**45**, 234–238.

HARADA, J., PEDERSEN, T. & BARNEA, Z. (1970). *Acta Cryst.* A**26**, 336–344.

HARDY, A.-M., HARDY, A. & FEREY, G. (1973). *Acta Cryst.* B**29**, 1654–1658.

HEILAND, G., KUNSTMANN, P. & PFISTER, H. (1963). *Z. Phys.* **176**, 485–497.

IEEE Standard on Piezoelectricity. (1978). IEEE Std 176-1978. Institute of Electrical and Electronics Engineers, New York, USA.

IHRINGER, J. & ABRAHAMS, S. C. (1984). *Phys. Rev. B*, **30**, 6540–6548.

International Tables for Crystallography. (1992). Vol. C. Dordrecht: Kluwer.

International Tables for Crystallography. (1994). Vol. D. In preparation.

ISO Guide to the Expression of Uncertainty in Measurement (1993). International Organization for Standardization, Geneva, Switzerland.

KARPINNEN, M., LIMINGA, R., KVICK, Å. & ABRAHAMS, S. C. (1988). *J. Chem. Phys.* **88**, 351–355.

KARPINNEN, M., LIMINGA, R., LUNDGREN, J.-O., KVICK, Å. & ABRAHAMS, S. C. (1986). *J. Chem. Phys.* **85**, 5221–5227.

KEVE, E. T., ABRAHAMS, S. C., NASSAU, K. & GLASS, A. M. (1970). *Solid State Commun.* **8**, 1517–1520.

KITTEL, C. (1971). *Introduction to Solid State Physics*, 4th ed. New York: Wiley.

KLASSEN-NEKLYUDOVA, M. V. (1964). *Mechanical Twinning of Crystals*. New York: Consultants Bureau. [Translation of a Russian language text with the same title published in 1960 by the Press of the USSR Academy of Sciences.]

LANDOLT-BÖRNSTEIN (1979). New Series, III/11, edited by K.-H. HELLWEGE & A. M. HELLWEGE. Berlin: Springer-Verlag. See also Supplementary III/18 (1984).

LANDOLT-BÖRNSTEIN (1981). New Series, III/16a, edited by K.-H. HELLWEGE & A. M. HELLWEGE. Berlin: Springer-Verlag. See also Supplementary III/28a (1990).

LANDOLT-BÖRNSTEIN (1984). New Series, Supplementary III/18, edited by K.-H. HELLWEGE & A. M. HELLWEGE. Berlin: Springer-Verlag.

LANG, S. B. (1971). *Phys. Rev. B*, **4**, 3603–3609.

LANG, S. B. (1974). *Sourcebook of Pyroelectricity*. New York: Gordon and Breach.

LE PAGE, Y., CALVERT, L. D. & GABE, E. J. (1980). *J. Phys. Chem. Solids*, **41**, 721–725.

LI, Y.-Y. (1981). *Ferroelectrics*, **35**, 167–172.

LIMINGA, R. & ABRAHAMS, S. C. (1976). *J. Appl. Cryst.* **9**, 42–47.

LINES, M. E. & GLASS, A. M. (1977). *Principles and Applications of Ferroelectrics and Related Materials*. Oxford: Clarendon Press.

LISSALDE, F., ABRAHAMS, S. C., BERNSTEIN, J. L. & NASSAU, K. (1979). *J. Appl. Phys.* **50**, 845–851.

LUNDGREN, J.-O., KVICK, Å., KARPPINEN, M., LIMINGA, R. & ABRAHAMS, S. C. (1984). *J. Chem. Phys.* **80**, 423–430.

MARBACH, H. (1856). *Ann. Phys. Chem.* **99**, 451–466.

MASON, W. P. & JAFFE, H. (1954). *Proc. IRE*, **42**, 921–930.

MEGAW, H. D. (1952). *Acta Cryst.* **7**, 187–194.

MILLER, R. C., ABRAHAMS, S. C., BARNS, R. L., BERNSTEIN, J. L. & NORDLAND, W. A. (1971). *Solid State Commun.* **9**, 1463–1465.

MOROSIN, B. (1972). Private communication, see Ref. 25 of Bergman & Crane (1974).

NASSAU, K., LEVINSTEIN, H. J. & LOIACONO, G. M. (1966). *J. Phys. Chem. Solids*, **27**, 989–996.

NYE, J. F. (1957). *Physical Properties of Crystals*. Oxford: Clarendon Press.

PERCIVAL, M. J. L. (1990). *Phase Transitions in Ferroelastic and Co-elastic Crystals*, edited by E. K. H. SALJE. Cambridge Univ. Press.

PERCIVAL, M. J. L., SCHMAHL, W. W. & SALJE, E. (1989). *Phys. Chem. Miner.* **16**, 569–575.

Properties of Lithium Niobate (1989). *EMIS Datareviews Series* No. 5. London: INSPEC.

RAMACHANDRAN, G. N. (1951). *Proc. Indian Acad. Sci.* **33**, 217–227; **33**, 309–315; **34**, 127–135.

RAVEZ, J., ABRAHAMS, S. C. & DE PAPE, R. (1989). *J. Appl. Phys.* **65**, 3987–3990.

RAVEZ, J., ANDRIAMAMPIANINA, V., SIMON, A., GRANNEC, J. & ABRAHAMS, S. C. (1991). *J. Appl. Phys.* **70**, 1331–1336.

RAVEZ, J., ANDRIAMAMPIANINA, V., SIMON, A., RABARDEL, L., IHRINGER, J. & ABRAHAMS, S. C. (1994). *J. Appl. Cryst.* **27**, 362–368.

RAVEZ, J., ARQUIS, S., GRANNEC, J., SIMON, A. & ABRAHAMS, S. C. (1987). *J. Appl. Phys.* **62**, 4299–4301.

ROSENZWEIG, A. & MOROSIN, B. (1966). *Acta Cryst.* **20**, 758–761.

SALJE, E. K. H. (1990). Editor. *Phase Transitions in Ferroelastic and Co-elastic Crystals*. Cambridge Univ. Press.

SCHWARZENBACH, D., ABRAHAMS, S. C., FLACK, H. D., GONSCHOREK, W., HAHN, T., HUML, K., MARSH, R. E., PRINCE, E., ROBERTSON, B. E., ROLLETT, J. S. & WILSON, A. J. C. (1989). *Acta Cryst.* A**45**, 63–75.

SHAY, J. L. & WERNICK, J. H. (1974). *Ternary Chalcopyrite Crystals: Growth, Electronic Structure, and Applications*. New York: Pergamon.

SHIOZAKI, Y. & MITSUI, T. (1963). *J. Phys. Chem. Solids*, **24**, 1057.

STADNICKA, K., GLAZER, A. M. & MOXON, R. J. (1985). *J. Appl. Cryst.* **18**, 237–240.

STÅHL, K., KVICK, Å. & ABRAHAMS, S. C. (1990). *Acta Cryst.* A**46**, 478–485.

SVENSSON, C. & ABRAHAMS, S. C. (1984). *J. Appl. Cryst.* **17**, 459–463.

SVENSSON, C., ABRAHAMS, S. C. & BERNSTEIN, J. L. (1979). *J. Chem. Phys.* **71**, 5191–5195.

SVENSSON, C., ALBERTSSON, J., LIMINGA, R., KVICK, Å. & ABRAHAMS, S. C. (1983). *J. Chem. Phys.* **78**, 7343–7352.

TOLÉDANO, J.-C. & TOLÉDANO, P. (1987). *The Landau Theory of Phase Transitions*. Singapore: World Scientific.